Nanoscale

Accepted Manuscript

Volume 10
Number 4
28 January 2018
Pages 1549-2172

Nanoscale

rsc.li/nanoscale

ISSN 2040-3372

PAPER
Shuping Xu, Chongyang Liang *et al.*
Organelle-targeting surface-enhanced Raman scattering (SERS) nanosensors for subcellular pH sensing

ROYAL SOCIETY OF CHEMISTRY

NCNST

ROYAL SOCIETY OF CHEMISTRY

rsc.li/nanoscale

Carbon dots-phthalocyanine hybrids: synergistic effects that boost their multifaceted applications

Carla I. M. Santos,[1,2]* Ana Catarina Almeida,[3] Ana L. F. Martins,[3] Ana R. Araújo,[2] Leandro M. O. Lourenço,[2]* Gil Gonçalves,[3,4]* M. Graça P. M. Neves[2]*

[1.] *Centro de Química Estrutural (CQE), Instituto Superior Técnico, Av. Rovisco Pais, 1049-001 Lisboa, Portugal.*

[2.] *LAQV-REQUIMTE, Department of Chemistry, University of Aveiro, Campus Universitário de Santiago, 3810-193 Aveiro, Portugal.*

[3.] *TEMA-Nanotechnology Research Group, Mechanical Engineering Department, University of Aveiro, Campus Universitario de Santiago, 3810-193 Aveiro, Portugal.*

[4.] *Intelligent Systems Associate Laboratory (LASI), 4800-058 Guimarães, Portugal.*

*Corresponding authors: carla.santos@tecnico.ulisboa.pt, leandrolourenco@ua.pt ggoncalves@ua.pt and gneves@ua.pt.

Abstract: Since their discovery, carbon dots (CDs) have been extensively studied for their potential in diverse applications owing to their unique properties such as high biocompatibility, excellent water solubility, low toxicity, minimal photobleaching, and exceptional chemical versatility. These characteristics position CDs as promising candidates for overcoming the limitations of various molecular compounds. This review provides a comprehensive analysis of the synergistic effects arising from the integration of CDs and phthalocyanines (Pcs) to form hybrids with distinct photophysical and photochemical properties. This study explores recent advances in the development of Pc@CDs hybrids, focusing on their synthesis, conjugation strategies, and synergistic effects that impact their performance in several areas, including optical sensing, electrocatalysis, photodynamic processes and photocatalysis. Emphasis is given to chemical methods that enable efficient conjugation and the role of reactive oxygen species generation in driving these applications. Additionally, the discussion also addresses key challenges, highlighting innovative solutions, and proposing future research directions to fully harness the potential of Pc@CDs hybrids in diverse scientific and technological breakthroughs.

Keywords: Carbon dots; Phthalocyanines; Pc@CDs hybrids; Covalent and non-covalent interactions; Photo- and electrochemical-based applications.

Nanoscale Accepted Manuscript

1. INTRODUCTION

1.1. Carbon Dots structure and properties

Carbon dots (CDs) are considered a new emerging class of zero-dimensional (0D) carbon-based luminescent nanomaterials. Although CDs have just recently gained notoriety, it is postulated that they should be one of the oldest and most abundant nanoparticles on earth resulting from natural phenomena such as combustion.[1],[2] Their denomination arises from the fact they are mainly composed of carbon in different types of hybridization states. Typically, CDs present a broad photoluminescent (PL) profile where the emission is extremely dependent on the excitation wavelength. The optical properties of the CDs are usually controlled by intrinsic structural features including the size and morphology, functional groups, and heteroatom doping. CDs are defined by size below 10 nm with a quasi-spherical morphology, that are composed of sp^2/sp^3 carbon core that can be easily doped with heteroatoms like boron, nitrogen, and/or sulfur.[3] Their surface usually presents abundant functional groups such as carboxyl, hydroxyl, amine, and/or polymer chains, depending on the raw material and synthesis method applied for their fabrication.[4] Although important pieces of the *puzzle* about the chemical structure of CDs have been uncovered, some critical knowledge remains unknown, owing to the complexity of the reaction pathways involved in their manufacture.[5] Consequently, the molecular origin and other key factors that control CDs photophysical properties are still, in most cases, an enigma that has been slowly revealed.[6] So far, it is well known that some properties can be mainly attributed to the CDs core, such as toxicity, while other properties can be mainly ascribed to surface functional groups, like dispersibility and optical properties.[7] [1]H and [13]C Nuclear Magnetic Resonance (NMR) has been recently explored as an essential tool for the identification of the functional groups of CDs, thanks to its accuracy in disclosing molecular species.[8] The impact of CDs on scientific research has been mostly associated with their extraordinary optical properties, including tuneable photoluminescence,[9] excitation-wavelength dependent emission,[10] and multiphoton excitation.[11–13]

The intense research on light-emitting CDs was sparked in 2006 with the discovery of room-temperature light emission.[14] The pioneer CDs presented emissions mostly located at the blue- or green-light region, however, the researchers recently developed new synthetic strategies to shift their emission to red- and near-infrared regions (therapeutic window) to improve their relevance for biomedical applications.[15–18] Nowadays, CDs can present a broad range of emission bands covering almost the full spectrum, including UV-Vis and infrared regions.[19–21]

The high versatility of chemical modifications of CDs is one of the most desirable nanostructures to face several technological challenges. Several strategies have been employed including,

heteroatom[22] or metal[23] surface passivation,[24] edge groups modification,[25] or organic functionalization.[6] Compared to heteroatom doping, surface functionalization, based on well-established organic reactions, is more controllable. Various approaches have been explored for the chemical modification of CDs including surface chemistry interactions (e.g., hydrophobic, electrostatic, and π-π interactions) or through the establishment of strong molecular bonds (e.g., covalent bonding) or interactions (e.g., coordination). The chemical surface modification of CDs can contribute to tuning solvents' dispersibility, induce desired biological targeting, regulate catalytic performance, improve the photoluminescence (PL) emission, and regulate the band gaps of CDs. These extraordinary features of CDs allowed their fast proliferation for the development of advanced novel materials that found relevant applications in several fields, including biomedicine, sensing, (photo)catalysis, electronics, energy, and environmental remediation. In addition, CDs present lower toxicity, minor production costs, and excellent biocompatibility, when compared with some traditional semiconductor inorganic quantum dots containing cadmium or lead.[26–29]

The extensive diversity of methodologies explored thus far, coupled with the wide array of available carbon-based raw materials, has led to an exponential growth in the preparation of various CDs types. The categorization of CDs is closely linked to the extent of carbonization and graphitization within their carbon core. Therefore, the synthetic parameters of CDs can be customized to achieve specific properties (**Figure 1 A**).
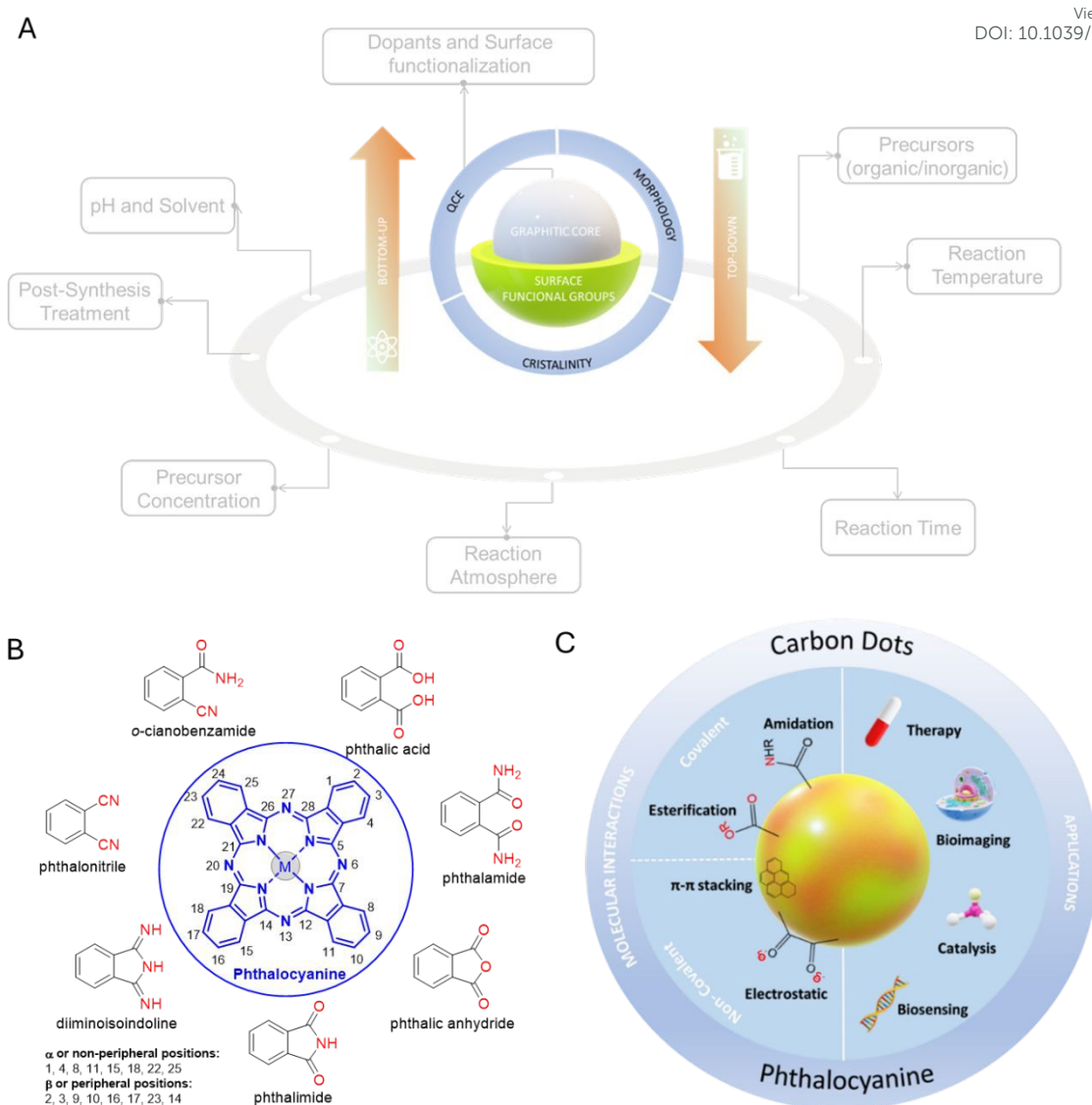
Figure 1. A key synthetic experimental parameters that influences the chemical, structural and optical properties of the CDs. Typical structure of CDs showing the graphitic core and surface functional groups, with an indication of the bottom-up and top-down synthesis. Indication of the main parameters used for CDs current classification: crystallinity, morphology, and quantum confinement effects (QCE). B Free-base phthalocyanine (M = 2H) and metallophthalocyanine (M = metal ion) structures prepared from the most common precursors. The nomenclature of phthalocyanine macrocycle is described according to IUPAC, the letters β and α indicate the peripheral and non-peripheral positions, respectively. C Left side: Overview of the different molecular interactions of CDs with Pcs, divided into covalent and noncovalent interactions. Right side: Overview of different applications of CDs linked to Pcs.

Effective control of the experimental parameters is critical for controlling the structure, morphology, and final properties of CDs. The first step in the design of CDs is to properly define the starting materials that can originate from organic or inorganic precursors. Organic

precursors, such as citric acid, glucose, or amino acids, tend to produce amorphous or quasi-graphitic CDs, whereas inorganic precursors might result in more graphitic CDs. The temperature at which synthesis occurs can significantly affect the degree of carbonization and graphitization. Higher temperatures often lead to more ordered graphitic structures, whereas lower temperatures induce the formation of amorphous carbon structures. The reaction duration is also an important parameter, with longer reaction times favouring more extensive carbonization and graphitization, resulting in CDs with a higher degree of crystallinity. The type of atmosphere (air, nitrogen, or argon) can also affect the carbonization process, where inert atmospheres such as nitrogen or argon can promote graphitization by minimizing oxidation. The concentration of the precursors, pH of the reaction solution, and choice of solvent can influence the reaction kinetics, and consequently, the structure of the CDs. The carbonization process can also be affected by the solvent type. The introduction of dopants or surface functional groups during the synthetic process can further modify the properties of CDs. Post-synthesis treatments, such as annealing or surface passivation, can be applied to modify the properties of CDs after synthesis. The diverse range of CDs reported in recent years has sparked vigorous debates regarding their classification and nomenclature. Consequently, the absence of well-defined parameters for standardization has resulted in similar CDs being referred to by different designations. As a result of this imprecise terminology, distinguishing between different types of CDs in literature has become a considerable challenge. To address this classification challenge, we will adopt the categorization proposed by Prato *et al.*,[5] which is based on three fundamental criteria: morphology, quantum confinement effects (QCE), and crystallinity (**Figure 1 A**). According to this classification, CDs can be divided into four primary subtypes. Graphene Quantum Dots (GQDs) feature a graphitic planar structure modified with chemical functional groups either at the edges or within interlayer defects. These functional groups are responsible for their intriguing quantum confinement effects and edge effects. GQDs typically have a higher ratio of sp^2 carbon atoms, resembling a few layers of graphene in their core, with the surface covered by sp^3 carbon atoms. Their QCEs are linked to the size of the emissive π domains. The Carbon Quantum Dots (CQDs) exhibit a spherical core-shell morphology, with a crystalline lattice containing a high density of sp^2 hybridized carbon atoms in the core and a shell intercalated typically with oxygen and nitrogen functional groups. These structural features result in quantum confinement effects within the emissive π domains. Carbon Nanodots (CNDs) are quasi-spherical nanoparticles characterized by a carbonized core structure and surface functional groups. Carbonized Polymer Dots (CPDs) typically possessing quasi-spherical morphologies, have hybrid structures comprised of sp^2, sp^3, or both sp^2 and sp^3 hybridized carbon atoms in their core. The surfaces are densely covered with polymer chains, and their

photoluminescence properties are primarily attributed to the crosslink-enhanced emission effect. Two major approaches can be found in the literature regarding the preparation of CDs: bottom-up and top-down approaches (**Figure 1 A**).[5,30–33]

The bottom-up approach typically explores molecular organic precursors, carbohydrates, and polymers as raw materials for the preparation of CDs. Most of the precursors, after being subjected to hydrothermal treatment, microwave (MW)-assisted synthesis, or pyrolysis, undergo partial dehydration and dehydrogenation before forming the CDs backbone structure.[34–37] Bottom-up methods are typically used to afford CPDs but have also been extensively used to prepare GQDs and CQDs. Usually, the preparation of CDs using this approach requires harsh reaction conditions, such as high temperature and pressure. In addition, it was reported that the addition of other chemical agents to the reaction medium, such as acids, can favor the formation of CDs.[38] The hydrothermal synthesis of CDs using organic precursors in a Teflon-lined autoclave has been one of the most explored bottom-up strategies owing to the simplicity of the experimental protocol. The basic premise of CDs formation consists of the reaction between the carbon precursors to form small graphitic structures upon heating. As mentioned above, the size and degree of carbonization of CDs can be effectively controlled by optimizing different reaction parameters, such as solvents, temperature, and reaction time.[39] The most explored precursor for the synthesis of CDs is citric acid (CA), which, in conjugation with different nitrogen-containing precursors, allows obtaining CDs with different optical features in a controlled manner.[40–42]

The top-down approach is characterized by the extensive fragmentation of carbon-based materials, whether they are in macro-, micro-, or nano-form, into tiny nanosized particles. This strategy typically employs carbon allotropes as raw materials, including graphite, carbon black, carbon fibers, carbon nanotubes (CNTs), carbon nanohorns (CNHs), fullerenes, and various graphene-based materials. The primary objective is to convert the large sp^2 carbon domains within these materials into smaller sp^2 domains, ultimately forming GQDs.[13] Consequently, following this conversion process, the inherent zero bandgap of the graphene structure transforms into a nonzero bandgap due to quantum confinement. This transformation was accompanied by an increase in edge defects, which played a crucial role in the properties of the resulting GQDs. The controlled process of fragmenting graphene can be achieved through several methods, including arc discharge, ball milling, laser ablation, chemical oxidation, and electrochemical etching.[43] In particular, the chemical oxidation of carbon nanostructures using MW or hydrothermal treatment has garnered significant attention for GQDs preparation. Among these methods, graphene oxide (GO) derivatives have emerged as a popular choice as

Nanoscale Accepted Manuscript

precursor materials for the top-down synthesis of GQDs.[44–46] The high oxidation state of GO nanosheets and their derivatives, characterized by randomly dispersed small sp² domains within an sp³ matrix, facilitates efficient chemical nanocutting. This process ultimately results in the formation of oxygen-doped GQD fragments with tunable optical properties.

The chemical structure of CDs plays a crucial role in mediating their functionalization, whether through covalent or non-covalent approaches. As mentioned, CDs possess various functional groups on their surface, such as amino, hydroxyl, and carboxyl, which improve their water stability and provide ideal sites for functionalization with ions, molecules, biomolecules, and polymers. Among these, amine and carboxyl groups are most commonly used for covalent conjugation with PCs through amide bond formation. The concentration of these functional groups on the CD surface typically determines the success and yield of the reaction. CDs can also undergo additional chemical modifications to increase the density of these functional groups. A common approach involves converting hydroxyl (-OH) groups to carboxyl (-COOH) groups, which is easily implemented through the reaction with chloroacetic acid under basic conditions.[46] Non-covalent conjugation of CD with PCs is another very explored approach for the synthesis of novel hybrid materials. The surface functional groups can facilitate electrostatic interactions with positively or negatively charged PCs, depending on the pH of the reaction medium. Another approach relies on π-π stacking or establishment hydrophobic interactions. In contrast to covalent conjugation, where a higher density of surface functional groups is beneficial, non-covalent conjugation is more effective when CDs have lower surface functionalization and larger aromatic domains.[32] Although the aromatic structure of CDs is highly dependent on the synthesis method, various reduction post-treatments have been explored to enhance their graphitic domains, thereby improving their conjugation efficiency with PCs.

However, it is important to note that the chemical structure of PCs can be tuned with complementary functionalization to enhance their covalent or non-covalent interactions with CDs.

1.2. Phthalocyanines structural features and synthetic approaches

Pcs are a class of macrocycles of synthetic origin that are structurally similar to analogous porphyrin derivatives, but with a core composed of four isoindole units linked through *aza* bridges (**Figure 1 B**). The term "phthalocyanine" (Pc) was suggested by Linstead, in 1933, to describe this type of blue-green pigments and results from the combination of the prefix *phthalo*, highlighting their synthetic origin from phthalic anhydride and derivatives, and *cyanine* due to their dominating blue color. However, the first reference to these blue-green derivatives appeared in 1907, when Tscherniak et al. noticed the formation of a small amount of a blue

compound after heating *o*-cyanobenzamide.[47] In 1927, Von der Weid et al. of the University de Fribourg described the formation of a highly stable blue material during the chemical reaction of 1,2-dibromobenzene with copper cyanide in pyridine reflux.[48–50] However, the compound was not correctly identified (molecular formula $C_{26}H_{18}N_6Cu$), [48] and only six years later (1933), Linstead reported the correct structure as being the free-base phthalocyanine **H₂Pc** and its Cu(II) complex **CuPc** (**Figure 1 B**). In the same period, *Scottish Dyes Ltd*. also detected a highly stable and insoluble blue impurity during their attempts to produce phthalimide from phthalic anhydride and ammonia, which was patented due to its economic interest, was posteriorly identified, namely by X-ray crystallography, as being the Fe(II) complex of phthalocyanine.[51–56] With this progress, synthetic routes were reported[57–60] and, in 1935, Cu(II) phthalocyanine was synthesized at an industrial scale and used as a blue pigment for the paint industry. Linstead investigations were encouraging, but in the case of other scientific areas, the insolubility of these pigments limited their use. In the 60s, the synthesis of highly soluble Pc derivatives allowed the diversification of the applications of these chromophores to other fields.[61–63] In the synthetic access to this type of macrocycle, a great variety of precursors can be used, such as *o*-cyanobenzamide, phthalic acid, phthalic anhydride, phthalimide, diiminoisoindoline, and phthalonitrile (**Figure 1 B**).[61,64] One of the most common precursors are phthalonitriles, which depending on the reaction conditions (e.g., reaction time, temperature, solvent, type of atmosphere, base, and catalyst selected)[65] are initially transformed into diiminoisoindoline derivatives *via* reaction with ammonia. This is followed by cyclotetramerization, usually in alcoholic solutions at high temperatures. It is noteworthy, that the reaction is favoured by the use of a catalytic organic base, such as 1,8-diazabicyclo[5.4.0]undec-7-ene (DBU) or 1,5-diazabicyclo[4.3.0]non-5-ene (DBN) in pentanol.[66–68] However, reactions with other precursors, such as phthalimide, phthalic acid, and phthalic anhydride, require urea as a nitrogen donor. To prepare free-base Pcs, lithium or magnesium is commonly used as a template, followed by demetallation of the obtained Pc complexes under dilute acidic conditions. On the other hand, the synthesis of metallophthalocyanines (**MPc**, M = metal ion) can involve two different approaches: i) the metal is inserted directly in the macrocycle during the tetramerization process using a phthalonitrile and an adequate metal salt;[69] ii) the metal is introduced in the previously prepared free-base **H₂Pc**, using an adequate metal salt carrier.[70] In the first approach, the access to metal complexes of Pcs requires the heating of the phthalonitrile derivative with the adequate metallic salt in a solvent with a high boiling point, such as dimethylaminoethanol (DMAE), *N,N'*-dimethylformamide (DMF) or 1-chloronaphthalene.[66] However, some procedures can be carried out at lower temperatures, by using a basic catalyst such as DBU in pentan-1-ol,[66] or even at room temperature by using lithium in DMAE.[71] These conditions are

Nanoscale Accepted Manuscript

also relevant to convert **H₂Pcs** adequately substituted at peripheral positions into different **MPcs** (M = Zn^{2+}, Mg^{2+}, In^{3+}, Ga^{3+}, Ge^{3+}, Si^{4+}, among others). Most Pcs applications are related to the delocalization of 18 π-electrons, leading to relevant physico-chemical and photophysical/photochemical features. In general, their electronic spectra present a broad band around 300-400 nm called the Soret band (S- band), and an intense Q-band located in the range of 600-750 nm. Moreover, the excitation of Pcs at a specific wavelength reveals a fluorescence emission between 600 and 800 nm. It is well established that the required features of a Pc for a special target application can be modulated through structural alterations at the peripheral α- and/or β-positions, leading to new systems with distinct characteristics, such as (photo)stability, water solubility, electron transfer abilities, suitable singlet oxygen ($^1O_2$) quantum yields (Φ_Δ), and fluorescence quantum yields (Φ_F). This is responsible for the unequivocal success of Pcs in several scientific areas, namely: i) biomimetic models of photosynthetic primary processes;[72] ii) catalysts[73,74] or photocatalysts;[73,75] iii) sensors;[70,76] iv) photosensitizers (PSs) for antimicrobial photodynamic therapy (aPDT) under different contexts: [77–80] v) PSs for photodynamic therapy (PDT) of malignant diseases,[81–83] vi) G-quadruplex aptamer binding,[84–86] and vii) markers in photomedicine.[87] More recently, the possibility of combining Pcs with different carbon-based nanostructures (e.g., CNTs, GO, or CDs),[88–90] to develop new conjugates with improved features for different applications has been an important focus of several research projects.

In this review, we will delve into a comprehensive discussion of various synthetic strategies employed to conjugate CDs with phthalocyanine (Pc) dyes through covalent and non-covalent interactions to obtain high-performance hybrids. The combination of these two entities has demonstrated remarkable synergistic effects, improved water solubility, and biocompatibility with promising outcomes in their applications as nanoprobes for sensing, electrocatalysts, and phototherapeutic agents. [91–95]

2. FUNCTIONALIZATION OF CARBON DOTS WITH PHTHALOCYANINES

CDs feature various functional groups on their surface, including amino, hydroxyl, and carboxyl units, which enhance their water stability and provide ideal anchoring sites for further functionalization. The chemical versatility of CDs enables them to establish a wide range of interactions with various types of ionic, molecular, and macromolecular entities *via* covalent and non-covalent interactions.[32] Interactions through covalent bonds require the presence of complementary functionalities in the Pcs and CDs. Since CDs can contain abundant carboxyl or amino groups on their surface, coupling mediated by amide bonds must be performed with Pcs bearing amino and carboxyl functionalities, respectively. In general, the esterification approach

involves the carboxyl groups of the CDs and hydroxyl groups present on the Pcs, whereas the sulfonylations require CDs functionalized with amino groups and Pcs with sulfonyl chloride functionalities. Most reported covalent strategies are based on amidation and esterification reactions (**Figure 1 C**). In the development of assemblies of Pc@CDs based on non-covalent bonds, their formation can occur *via* electrostatic, complexation, or π–π interactions (**Figure 1 C**). These interactions are mainly governed by the inverse surface charges between Pcs and CDs, or by the strong quenching promoted by the aromatic nature of Pcs and CDs.

In this review, we delve into a comprehensive discussion of the various strategies employed to covalently and non-covalently conjugate CDs with Pc dyes. The combination of these two entities has demonstrated remarkable synergistic effects, including alterations in the fluorescence quantum yield values (ϕ_f), generation of oxidative species, and improved water solubility and biocompatibility. In recent years, these intriguing Pc@CDs nanoconjugates have primarily been applied as nanoprobes for biosensing, electrocatalysts, antibacterial and phototherapeutic agents.[91,93,96,97] The current section is organized according to the type of interaction involving both components in the hybrid, non-covalent or covalent; this will be preceded by a brief reference concerning their impact on the final features of Pc@CDs. In each section, and when possible, the studies will be organized by their application or potential envisaged. Next, we present a detailed discussion of the properties and applications of Pc@CDs conjugates based on their non-covalent or covalent nature. Importantly, the inconsistent nomenclature used for CDs in the literature poses a significant challenge in distinguishing between the different types of CDs. To avoid potential misunderstandings, we will use the generic term "CDs" to refer to this class of carbon-based nanomaterials.

2.1. Non-covalent functionalization: electrostatic and/or π–π interaction

2.1.1. Fundamental insights into Pc@CDs features

The luminescence properties of CDs are extremely dependent on the type of chemical or physical interactions occurring at their surfaces and edges with other molecules that can enhance or quench fluorescence. Since CDs can act as energy donors and as electron donors the fluorescence quenching can occur *via* Förster resonance energy transfer (FRET) or by a photo-induced electron transfer (PET) process.[93,98,99] Achadu *et al*. reported, in 2015, a study that can be considered an important basis for further advancements involving Pc@CDs.[100] Based on the electron-donating characteristics of CDs and the behavior of MPcs to act either as electron donors or acceptors, prompted the authors to evaluate, for the first time, the fluorescence performance of the **ZnPc1@CDs** and **ZnPc2@CDs** conjugates (**Figure 1 A**), obtained by the

adsorption of **ZnPc1** and **ZnPc2** to CDs surfaces through electrostatic and π–π interactions, respectively. The CDs were prepared by the oxidation of GO in concentrated H_2SO_4 and HNO_3 under top-down hydrothermal conditions. The zinc(II) phthalocyanines bearing four pyridyloxy substituents (**ZnPc1a**) and bearing four carboxyphenoxy substituents (**ZnPc2**) were obtained by cyclotetramerization of the adequate phthalonitriles (4-(4-pyridyloxy)phthalonitrile **(Pht1)** and 4-(p-carboxyphenyloxy)phthalonitrile (**Pht2**), respectively) in pentan-1-ol in the presence of zinc(II) acetate in 1,8-diazabicyclo[5.4.0]undec-7-ene (DBU) or DMF.[101,102] Both phthalonitriles (**Pht1** and **Pht2**) were obtained through a nucleophilic ipso-nitro substitution reaction involving the commercially available 4-nitrophthalonitrile and 4-hydroxypyridine or 4-hydroxybenzoic acid, respectively, in the presence of K_2CO_3. Access to the cationic phthalocyanine **ZnPc1** required an extra step with the quaternization of the pyridyl units of **ZnPc1a** using methyl iodide.
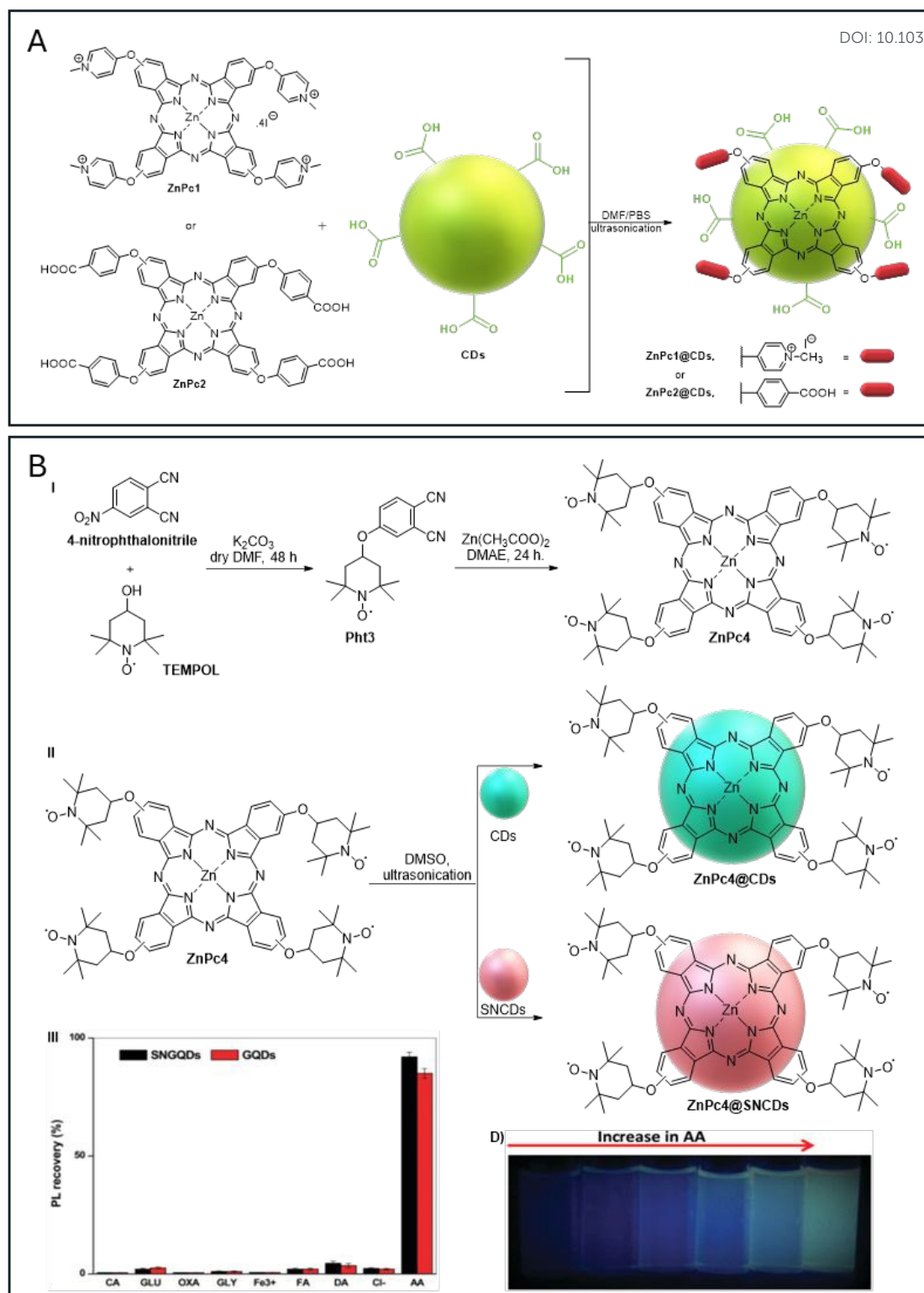
Nanoscale Accepted Manuscript

Figure 2. **A ZnPc1@CDs** and **ZnPc2@CDs** obtained via ionic and π–π stacking interactions with CDs. [100] **B I)** Synthesis of **ZnPc4** and hybrids **II) ZnPc4@CDs** and **ZnPc4@SNCDs**. **III)** Graphic with selective screening of different biomolecules and metal ions and their effects on the fluorescence response of 0.5 mg mL^{-1} of the **ZnPc4@CDs** and **ZnPc4@SNCDs** nanoprobes in DMSO. The concentration of AA was 20 nM and of the interfering ions 250 nM. Citric acid (CA); glucose (GLU); oxalic acid (OXA); glycine (GLY); dopamine (DA); folic acid (FA). **IV)** Fluorescence image of "turn ON" of CDs emission upon the addition of increasing concentration of AA (0–50 nM) to the probe solution viewed under UV light of 365 nm. Reproduced from Ref.[103] with

permission from the Centre National de la Recherche Scientifique (CNRS) and the Royal Society of Chemistry.

The **ZnPc1@CDs** was obtained by the addition of CDs in phosphate-buffered saline (PBS) solution at pH = 9 to the cationic **ZnPc1** in a DMF/PBS solution, followed by ultrasonication; the alkaline conditions were selected to favor electrostatic interactions between the negatively charged CDs and the positively charged **ZnPc1** (**Figure 2 A**). The hybrid **ZnPc2@CDs** was obtained under similar conditions, but at pH = 7, to minimize electrostatic repulsion and to favor π-π interactions. The extensive evaluation of the photophysical properties of the resulting hybrid materials allowed to conclude that the quenching of the CDs fluorescence in the hybrids when compared with that of CDs alone (Φ_F = 0.22 *versus* ca 0.18 for **ZnPc1**,**2@CDs**) is due to FRET; this conclusion was also supported by an improvement on the emission of the nearby ZnPc acceptors after excitation at 340 nm where the CDs absorb. The low FRET efficiency obtained for both hybrids (**ZnPc1** = 0.18 and **ZnPc2** = 0.14) was justified by the low spectral overlap between the emission of the donors (CDs) and the absorption of the acceptors (ZnPc derivatives). In the same work, the authors found that the covalent attachment of a Zn(II) tetraaminophthalocyanine (**ZnTAPc = ZnPc3**) to the CDs resulted also to a reduction in the fluorescence (Φ_F = 0.12), although the FRET efficiency was higher (Φ_F = 0.45). This behavior was attributed to the closeness of both components and their stronger interactions. Since other mechanisms such as electron transfer or exciton annihilation could also lead to fluorescence quenching, further experimental investigations, such as time-resolved fluorescence spectroscopy or a detailed energy level analysis, would help clarify other contributions to the quenching of the CDs fluorescence in the presence of ZnPcs.

2.1.2. Sensing applications

The possibility of exploring conjugates based on Pcs and CDs as nanoprobes for different analytes has attracted considerable attention from the scientific community. In this context, the noncovalent assembly of **ZnPc4** bearing 2,2,6,6 tetramethylpiperidin-1-yl)oxyl (**TEMPOL**) units with pristine **CDs** and **CDs** co-doped with S and N (**SNCDs**) were explored to assess their potential as fluorescence nanoprobes for the recognition of ascorbic acid (AA)(**Figure 2B**).[103] The selection of TEMPOL was motivated by the high selectivity and specificity of AA for paramagnetic TEMPO derivatives, leading to their conversion into diamagnetic hydroxylamine counterparts. The **ZnPc4** was obtained through cyclotetramerization of **Pht3** bearing the radical scavenger TEMPOL unit in DMAE and anhydrous $Zn(CH_3COO)_2$;[104] the **Pht3** was prepared from the condensation of commercially available 4-nitrophthalonitrile with TEMPOL under basic conditions to favor the required nucleophilic ipso-nitro substitution reaction. In this work, the

authors selected the hydrothermal treatment of citric acid with NaOH at 160 ºC to obtain pristine **CDs**, while the **SNCDs** were obtained under the same conditions but the NaOH was substituted by thiourea.[105] The non-covalent conjugation *via* π-π stacking interactions of **CDs** and **SNCDs** to **ZnPc4** after ultrasonication in dimethyl sulfoxide (DMSO) was confirmed using Fourier transform infrared (FTIR), Raman, and ultraviolet-visible (UV-Vis) spectroscopies.[103]

The photophysical studies revealed that the ΦF and lifetime (τf) of CDs decreased significantly upon conjugation with **ZnPc4** (**Table 1**) due to Förster resonance energy transfer (FRET). The higher FRET efficiency observed for **ZnPc4@SNCDs** (0.92) compared to **ZnPc4@CDs** (0.66) was attributed to a better spectral overlap (*J*). The donor–acceptor distances (8.1 and 9.2 nm) confirmed effective energy transfer within the 1–10 nm range. Titration assays with ascorbic acid (AA) restored the fluorescence of CDs and SNCDs ("turned ON"), suggesting that AA acted as a spacer or radical scavenger (**Figure 2 B**). The absence of an enhanced permeation retention (EPR) signal in the paramagnetic nanoassembly further supported this last mechanism. The nanoprobes exhibited high selectivity for AA, with detection limits of 0.2 nM (**ZnPc4@SNCDs**) and 0.8 nM (**ZnPc4@CDs**), and excellent specificity against biomolecules and metal ions (e.g., citric acid, glucose, dopamine, folic acid, Fe^{3+}, or Cl^-) (**Figure 2 B**). Their application in real sample quantification yielded near-quantitative recoveries, while the spectra of free **CDs** and **SNCDs** remained unchanged in the presence of AA.

The ability of maleimide units to react specifically with thiols *via* Michael addition[106] prompted Achadu *et al*. to develop **ZnPc5@CDs** nanoassemblies (**Figure 3 A**) to evaluate their potential as nanoprobes of biothiols (e.g., cysteine, homocysteine, or glutathione);[107] these derivatives, which are involved in several biological processes are increasingly recognized as potential biomarkers for certain diseases. The required **ZnPc5** was synthesized by reacting Zn(II) tetraaminophthalocyanine (**ZnPc3**) with maleic anhydride (**Figure 3 A**). Pristine CDs were obtained by oxidizing GO in H_2SO_4 and HNO_3. The fluorescence quenching observed in the **ZnPc5@CDs** nanoassemblies was attributed to maleimide attachment. For comparison, maleimide carbon dots (**M@CDs**) were prepared by reacting polyethyleneimine-grafted CDs (**PEI-CDs**) with 4-maleimidobenzoic acid, resulting in a "turn-OFF" state. However, the photoluminescence (PL) intensity of both nanoassemblies was gradually restored upon addition of cysteine, homocysteine, or glutathione but was not affected by the presence of several α-amino acids and proteins. **M@CDs** showed higher sensitivity than **ZnPc5@CDs**, due to the direct covalent attachment of maleimide units. No significant fluorescence increase occurred with non-immobilized **ZnPc5** upon adding cysteine, highlighting the key role of CDs in the "Turn ON"

Nanoscale Accepted Manuscript

behavior. However, to complement these studies, a comparison with **ZnPc3**-based nanoassemblies could provide a more realistic idea of the maleimide role in these hybrids.
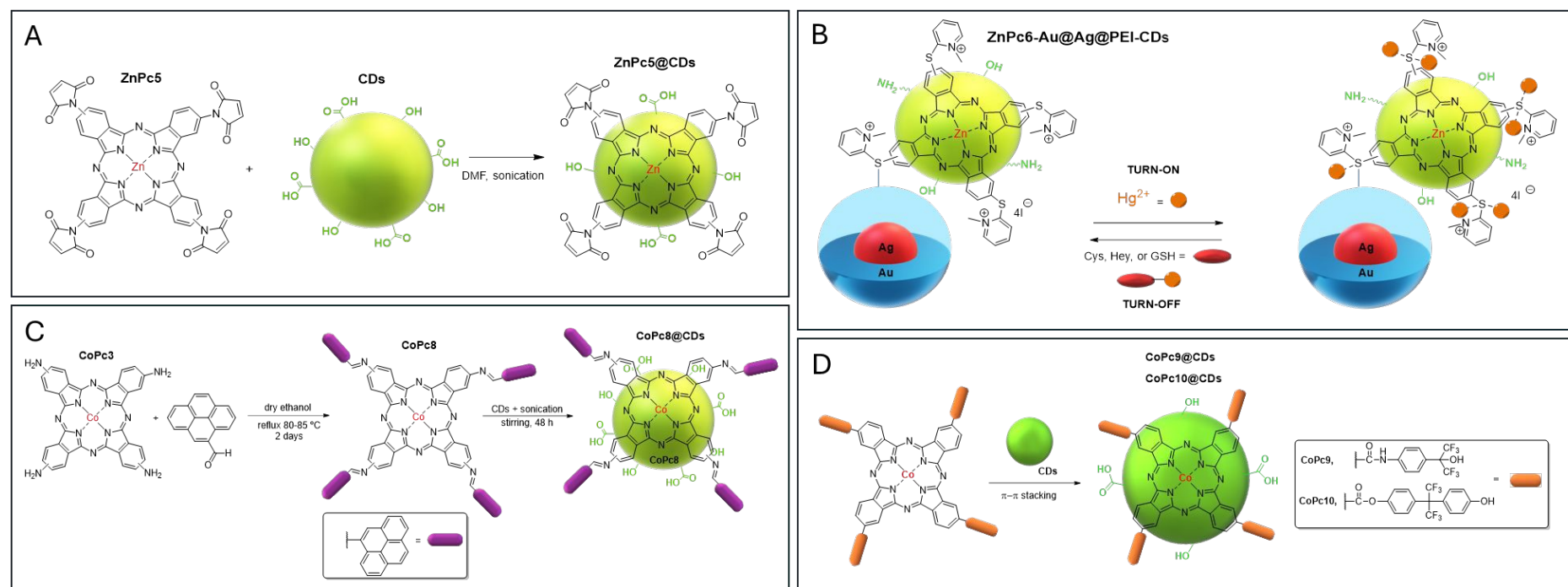
Nanoscale Accepted Manuscript

Figure 3. A Representation of the **ZnPc5@CDs** nanoassemblies.[107] **B** Proposed mechanistic actuation of the "Off-On-Off" nanoprobe **ZnPc6-Au@Ag@PEI-CDs** for the detection of Hg^{2+} and biothiols in aqueous solutions.[108] **C** Synthetic route for pyrene-derivatized **CoPc8** and **CoPc8@CDs** hybrids.[109] **D** Structures of **CoPc9** and **CoPc10** used for the preparation of **CoPc9,10@CDs** hybrids.[110,111]

In the same period, Nyokong *et al.* developed a dual fluorescence nanoprobe, **ZnPc6** **Au@Ag@PEI-CDs** (**Figure 3 B**), for detecting Hg^{2+} and biothiols in aqueous solution.[108] The sensing platform was assembled by electrostatically combining cationic **ZnPc6** bearing four thiopyridinium units with a nano-alloy **Au@Ag**, followed by embedding the conjugate in **PEI-CDs** obtained from a hydrothermal treatment of GO with hyperbranched polyethyleneimine. The nanoprobe's fluorescence emission was restored in the presence of Hg^{2+} and "turned OFF" upon the addition of biothiols, due to their ability to form strong Hg-S bonds (**Figure 3 B**). These "off-on-off" nanoprobes were stable and selective, with high resistance to interference from other amino acids (glycine, lysine, histidine, tryptophan, or DL-lactic acid) and metal ions (e.g., Fe^{2+}, Co^{2+}, Mn^{2+}, Cd^{2+}, Cu^{2+}, Ni^{2+}, Pb^{2+}, Mg^{2+}, Ag^+, and Zn^{2+}). Their effectiveness was confirmed in real samples spiked with test analytes.

A similar concept was considered in the design of "turn-ON" nanoprobes for detecting Hg^{2+}, obtained through the conjugation of CDs with **ZnPc6**, the corresponding Al(III) complex **AlPc6**, **ZnPc7** with eight thiopyridinium moieties, and the neutral **ZnPc6a.** [108] The fluorescence of the CDs, derived from GO via a hydrothermal method, was initially quenched upon coordination with the Pcs. However, in the presence of Hg^{2+}, the fluorescence was restored due to Hg^{2+}'s strong affinity for the mercapto bridges on the Pcs, which disrupted the π-π stacking interaction between the CDs and Pcs. These nanoprobes exhibited high selectivity for Hg^{2+} over other metal ions, with the best limit of detection (LOD) achieved by the octacationic **ZnPc7** (0.12 nM), followed by the tetracationic ones **ZnPc6** (LOD = 0.52 nM) and **AlPc6** (LOD = 0.60 nM). The performance was less effective for the neutral **ZnPc6a**, confirming the relevance of electrostatic interactions in the development of these nanoassemblies.

Achadu *et al*. described the synthetic access to the functional hybrid **CoPc8@CDs** (**Figure 3 C**) and demonstrated its use as a selective "turn ON" nanoprobe for CN^-.[109] The CDs were synthesized by a top-down hydrothermal process, and the Schiff complex **CoPc8** was obtained by coupling the tetraamino cobalt(II) phthalocyanine **CoPc3** with 1-pyrene-1-carboxyaldehyde. The nanoassemblies obtained upon its conjugation with the CDs showed a typical "turn OFF" behaviour.

The sensing studies showed that in the presence of the anion cyanide, the CDs emission was restored and increased linearly with the concentration of CN^- (ranging between 1 nM and 50 nM) with a LOD of 0.5 nM. The probe's selectivity for CN^- was confirmed through fluorescence recovery assessments in water samples containing various anions (e.g., F^-, Cl^-, Br^-, I^-, $H_2PO_4^-$, HSO_4^-, NO_3^-, ClO_4^-, SCN^-, AcO^-, HSO_3^-, SO_4^{2-}, and CO_3^{2-}). The inefficacy of the analogous **ZnPc8**

complex in anion detection supports the hypothesis that axial coordination between the Co metal ion in the Pc inner core and CN⁻ was responsible for disrupting the initial donor-acceptor "turn OFF" behavior. Considering this fact, to evaluate the real role of the pyrene units in Pc, it would be interesting to compare the sensing results obtained with the nanoassemblies obtained from tetraamino cobalt(II) phthalocyanine **CoPc3** or even with non-substituted **CoPc**. The efficiency of this probe in evaluating trace levels of CN⁻ ions in a real context was confirmed using tap water spiked with known concentrations of CN⁻ between 0.5 – 50 nM with percentage recoveries higher than 97%.

The efficiency of Pc@CDs hybrids for gas detection, namely at room temperature, is also attracting some attention. In 2021, Jiang *et al*. developed nanoassemblies from CDs and CoPc dyes containing hexafluoroisopropanol (HFIP, **CoPc9**) and hexafluorbisphenol A (6FBPA, **CoPc10**) substituents (**Figure 3 D**), and explored their efficiency as sensors towards the chemical warfare agent simulant dimethyl methylphosphonate (DMMP).[110] The **CoPc9,10@CDs** hybrids showed strong hydrogen bonds between the two functional units (HFIP and 6FBPA) and the DMMP molecule, leading to an exceptional response behaviour to the analyte. Moreover, it has been reported that the CDs improved the electrical conductivity of the hybrids by π–π interactions with the CoPcs and can be considered promising raw materials for use in sarin gas sensors.

In 2021, Zhi Yang *et al*. developed hybrid materials for NO_2 gas sensing based on the anchorage of CDs onto the surface of **MPc11** (where the Pc is 2,9,16,23-tetracarboxylicphthalocyanine and M = Co, Ni, Cu, or Zn) nanofibers *via* π–π stacking interactions to form a charge transfer conjugate.[111] The addition of CDs greatly increased the conductivity of the Pc fibers, leading to a faster response of the hybrid materials up to 14.5 nA. The sensing mechanism is based on the typical p-type semiconductor behaviour of **MPc11@CDs**, which have a strong affinity for the electron acceptor molecule NO_2. Consequently, after the reaction with the complex, the electrons are trapped by NO_2, producing NO_2^- ions and holes in the nanofiber surface, significantly changing the conductivity of the sensors. The gas-sensitive response (I–V curves) of the **CoPc@CDs** hybrid material to 50 ppm NO_2 gas was nearly 16 times higher compared with the individual components. Moreover, the reproducibility, selectivity, and stability of the hybrids are significantly enhanced. The response value was achieved within 100 s, and the recovery curve reached the baseline 125 s after laser exposure.

In the context of biosensing applications, Santiago *et al.* reported in 2022, that the **ZnPc12@NCDs** and **ZnPc13@NCDs** nanoprobes (**Figure 4 A**) can induce on nitrogen doped carbon dots (NCDs) an "off-on" fluorescence behaviour, after interaction with the double-stranded DNA (ds-DNA). These nanoprobes were obtained from the positively charged **ZnPc12**

and **ZnPc13** and NCDs prepared by the hydrothermal treatment of GO in the presence of NH$_4$OH

and H$_2$O$_2$.[112] The ZnPcs were synthesized using the conventional tetramerization of suitable

phthalonitriles bearing one or two thiopyridyl units in DMAE and the presence of Zn(OAc)$_2$,

followed by quaternization of the pyridine units with CH$_3$I. Supramolecular **Pc@NCDs** hybrids

were prepared in water using solutions of NCDs and Pcs in a molar ratio of 1:5. This conjugation

promoted quenching of the emission of NCDs, but in the presence of ds-DNA, their

photoluminescence was restored. This behaviour was justified by the preferential interaction

between the positively charged Pcs and the negatively charged dsDNA, with the consequent

restoration of the NCDs photoluminescence. The obtained limits of detection for ds-DNA with

ZnPc13 and **ZnPc12** were 66 nM bp and 1.1 mM bp (bp = molar concentration of pairs),

respectively. The concentration difference used for each Pc dye is most likely associated with

their solubility, depending on the number of peripheral substituents (four *versus* eight). Both

nanosensors exhibit good selectivity for ds-DNA when tested against biothiols and inorganic
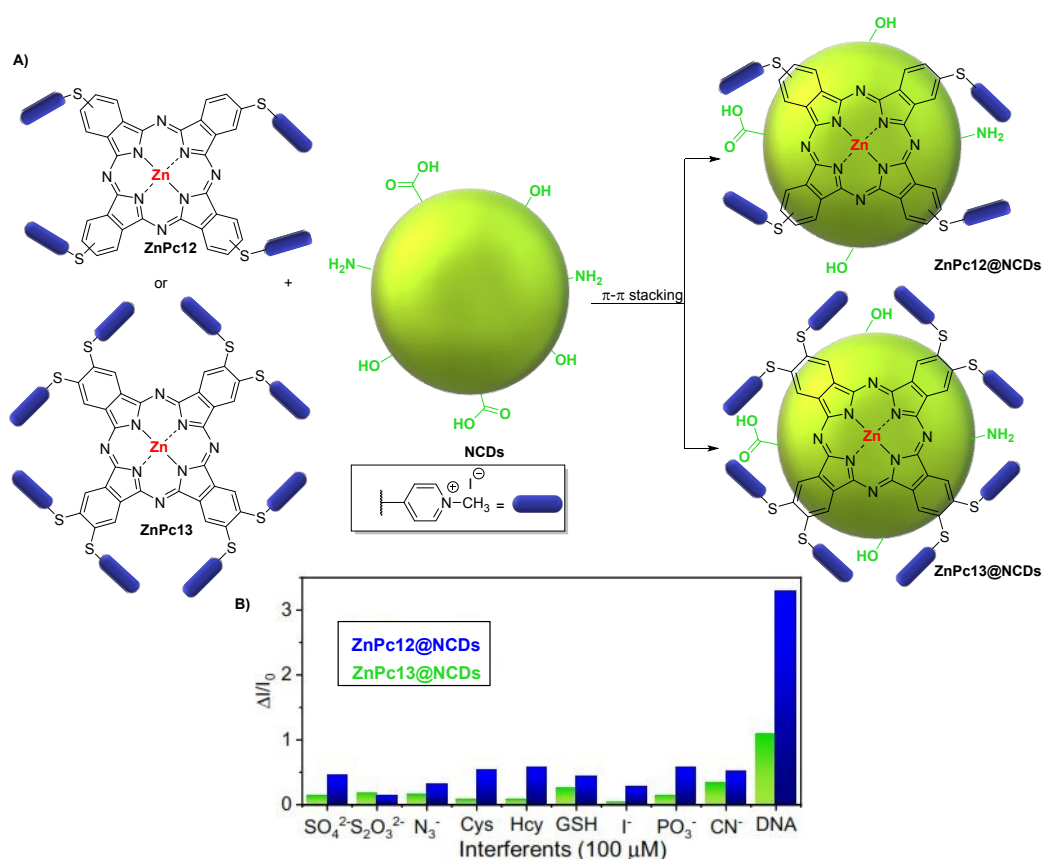
anions as potential interferents (**Figure 4 B**).

Figure 4. A Structures of the **ZnPc12,13** used in the formation of **ZnPc12,13@NCDs** nanohybrids.
B Selectivity of the nanosensors (**ZnPc12@NCDs** and **ZnPc13@NCDs** with 1:5 ratio of Pc:NCDs
and [NCDs] = 2 μM) towards ds-DNA, showing photoluminescence enhancement in the presence
of an excess (100 μM) of the various relevant analytes. Reproduced under terms of the CC BY
4.0 license. [112] Copyright 2022, MDPI.

Table 1. Summarized properties of **Pc@CDs** conjugates for sensing applications.

CD type	Chemical conjugation	Phthalocyanine	$\Phi_{f\ CDs}$	$\Phi_{f\ Pc}$	$\Phi_{f\ Hybrid}$	Application	Ref
SNCDs	Non-covalent (π-π stacking)	2,9(10),16(17),23(24)-Tetrakis[(4-methylpiperidin-1-yl)oxyl]phthalocyaninatozinc(II) (**ZnPc4**)	SNCDs (0.81)[a]	*	ZnPc4@SNCDs (0.15)[a]	Ascorbic acid detection	[103]
CDs			CDs (0.22)[a]	*	ZnPc4@CDs (0.09)[a]		
CDs	Non-covalent (π-π stacking)	2,9(10),16(17),23(24)-Tetrakis(1-pyrrolidine-2,5-dione)phthalocyaninatozinc(II) (**ZnPc5**)	CDs (0.31)[b]	ZnPc5 (0.2)[a]	ZnPc5@CDs (0.10)[b]	Biothiol detection (cysteine, homocysteine, or glutathione)	[107]
PEI-CDs			PEI-CDs (0.88)[c]		*		
M-CDs			MCDs (0.06)[b]	*	*		
PEI-CDs	Non-covalent (π-π stacking)	2,9(10),16(17),23(24)-Tetrakis(2-pyridiniumsulphanyl)phthalocyaninatozinc(II) Tetraiodide (**ZnPc6**)	PEI-CDs (0.68)[b]	*	ZnPc6-Au@Ag@PEI-CDs (0.10)[b]	Biothiol and Hg²⁺ detection	[108]
PEI-CDs-Au@Ag			PEI-CDs-Au@Ag (0.25)[b]				
NCDs	Non-covalent (electrostatic interactions)	2,9(10),16(17),23(24)-Tetrakis(4-pyridiniumsulphanyl)phthalocyaninatozinc(II) Tetraiodide (**ZnPc 12**) 2,3,9,10,16,17,23,24-Octakis(4-pyridiniumsulphanyl)phthalocyaninatozinc(II) Octaiodide (**ZnPc 13**)	NCDs (0.10)[d]	ZnPc12 (0.18)[a] ZnPc13 (0.21)[a]	*	ds-DNA detection	[112]
CDs	Non-covalent (π-π stacking)	2,9(10),16(17),23(24)-Tetrakis(2,6-di-*tert*-butyl-4-methylphenoxy)phthalocyaninatozinc(II) (**CoPc8**)	CDs (0.31)[a]	*	*	Cyanide ion detection	[113]

[a]DMSO, [b]PBS, [c]DMSO:PBS mixture, and [d]H$_2$O.

2.1.3.   Photosensitizing applications

Molecules, commonly known as PSs, that generate reactive oxygen species (ROS) upon excitation with visible light, are particularly relevant in various applications, including PDT, aPDT, and photocatalysis. Pc-based compounds, in particular, are recognized as promising candidates owing to their high efficiency to generate ROS, namely $^1O_2$ species.

Despite these advantageous properties, the low solubility of Pcs in aqueous media and their lack of specificity pose significant challenges for their biological applications. To overcome these limitations, researchers have investigated the conjugation of Pcs to carbon-based nanomaterials. Among these, CDs have emerged as an appealing choice because of their high biocompatibility, water solubility, and efficient cellular internalization.[114,115] The following sections discuss various approaches reported in the literature for synthesizing Pc-based CDs assessing their performance in terms of emission quantum yield and ROS generation. Such insights are crucial for advancing solutions involving PSs, particularly Pcs. These applications include tumour cell eradication, microorganism inactivation and photocatalysis, underscoring the diverse potential of Pc@CDs in photosensitizing processes.

2.1.3.1. Cancer therapy

To identify efficient Pc@CDs hybrids for phototherapeutic applications, Matshitse *et al.* evaluated how the physicochemical features of the obtained nanoassemblies through electrostatic and/or π–π interactions were affected by the Pc charge. This systematic study was performed using unsubstituted **ZnPc**, **ZnPc1** bearing *N*-methylpyridyloxy units, and the tetrasulfonated **ZnPc14** as prototypes, respectively, of neutral, positively, and negatively charged derivatives to construct the corresponding CDs nanoassemblies (**Figure 5 A**).[116] CDs with a size near 2.2 nm were obtained through the chemical oxidation of GO using $KMnO_4$ and H_2SO_4 as oxidative agents.[117] The successful conjugation was confirmed by different characterization techniques, and it was concluded that the largest loading was observed for **ZnPc1@CDs** (14 Pc molecules per CD *versus* 4 for **ZnPc** and 3 for **ZnPc14**). These results were attributed to the establishment of both π–π and electrostatic interactions between the negatively charged CDs and the positively charged **ZnPc1**.
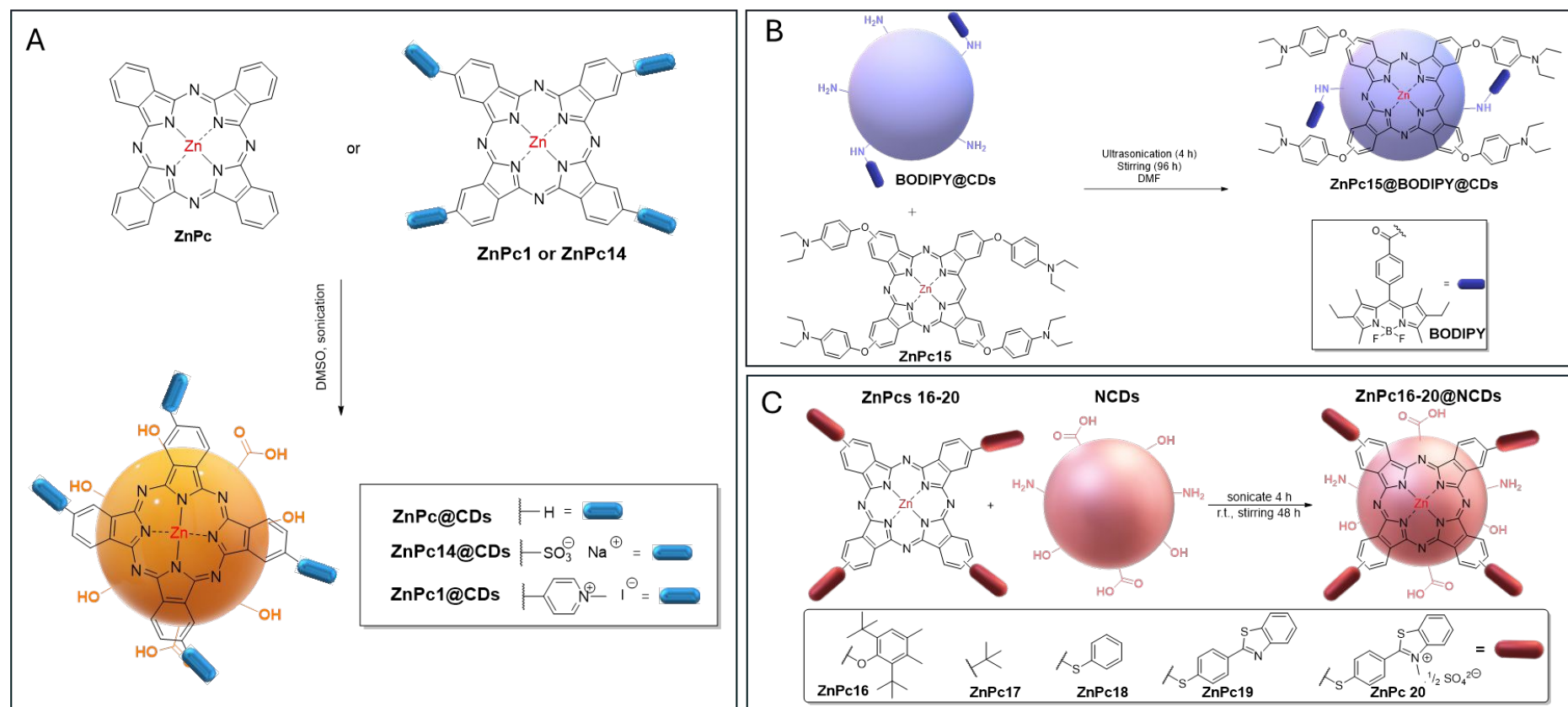
Figure 5. A The structures of neutral, negatively charged, and positively charged Pc dyes used to evaluate the impact of charge type on the physicochemical features of ZnPc@CDs. [116] **B** Formation of **ZnPc15@BODIPY@NCDs** conjugates *via* covalent conjugation of NCDs with BODIPY and subsequent π-π interactions with **ZnPc15**. [118] **C** Structures of **ZnPc16-20** for the preparation of **ZnPc16-20@NCDs** *via* π-π interactions. [119]

22

The results showed that the Φ_F of CDs in DMSO decreased from 11% to 2% upon conjugation to **ZnPc1** and **ZnPc**, and to ~8% for **ZnPc14**. This quenching was accompanied by a decrease in τ_f. The smaller quenching observed for **ZnPc14@CDs** was attributed to its lower loading, reducing aggregation. FRET efficiency analysis indicated a strong energy transfer for **ZnPc@CDs** (0.81) and **ZnPc1@CDs** (0.80), while **ZnPc14@CDs** had a lower efficiency (0.28) due to electrostatic repulsion increasing donor-acceptor distance (**Table 2**). **ZnPc1@CDs** showed the highest FRET efficiency due to attractive interactions between oppositely charged surfaces. Despite increased triplet quantum yields (Φ_T) upon conjugation, this increase was not reflected in the Φ_Δ values of the hybrids that remained lower than that of ZnPc alone ($\Phi_\Delta = 0.67$) or similar to the free **ZnPc1** ($\Phi_\Delta = 0.41$) and **ZnPc14** ($\Phi_\Delta = 0.32$). This fact was attributed to a screening effect preventing efficient energy transfer to the ground-state of molecular oxygen. Additionally, the presence of water further quenched $^1O_2$, contributing to their lower $\Phi\Delta$ values, when measured in this solvent.[106]

To evaluate how the size of CDs could affect the ability of Pcs to generate $^1O_2$, motivated Matshitse *et al.* considered the development and the photophysical/photochemical characterization of assemblies based on cationic **ZnPc1** and CDs with different sizes denominated as CD_2 (2.6 nm), CD_6 (3.3 nm), and CD_{10} (5.1 nm).[120] These CDs were prepared via the chemical cutting of GO using $KMnO_4$ and H_2SO_4 as oxidative agents and varying the reaction time from 2 to 6 h.[117] The results showed that the atomic concentrations of oxygen decreased with increasing sizes of CDs leading to a blue shift in their spectra and can justify the smaller Pc loading found for this assembly (3 versus 10 for **ZnPc1@CDs$_{10}$** and **ZnPc1@CDs$_2$** and 5 for **ZnPc1@CD$_6$**). Compared with the initial **ZnPc1** ($\Phi_\Delta = 0.03$), the presence of CDs improved the Φ_Δ values in water, with the best performance observed for **ZnPc1@CD$_6$** ($\Phi_\Delta = 0.27$), followed by **ZnPc1@CD$_2$** ($\Phi_\Delta = 0.17$) and **ZnPc1@CD$_{10}$** ($\Phi_\Delta = 0.11$). The low performance of **ZnPc1@CD$_2$** with the highest number of Pcs was attributed to the aggregation effects. This study showed that the structural features of CDs, namely, size, amount of oxygen, and the presence of Pc, can have an important impact on their phototherapeutic or photocatalytic applications.

In 2018, Nyokong *et al.* reported the synthesis of supramolecular hybrids constituted by the **ZnPc15** bearing diethylaminophenoxy substituents embedded in nitrogen CDs covalently linked through an amide bond to a carboxylic acid borondipyrromethane (**BODIPY@NCDs**) (**Figure 5 B**).[118] The photophysical characterization of the **ZnPc15@BODIPY@NCDs** hybrids showed a slight decrease in both the Φ_F and τ_F when compared with the CDs alone (0.23 and 2.84 ns *versus* 0.27 and 3.41 ns). The decrease in Φ_F values could be due to the FRET behaviour. Regarding $^1O_2$

production, **ZnPc15@BODIPY@CDs** (Φ_Δ = 0.70) displayed an improved $^1O_2$ generation ability compared to **ZnPc15** (Φ_Δ = 0.50) in DMSO.

In 2019, Nene *et al.* evaluated for the first time the phototherapeutic efficiency of conjugates obtained from a series of ZnPcs (**ZnPc16**-**20**) with CDs on human breast cancer MCF-7 cell lines (**Figure 5 C**).[119] The nitrogen-doped CDs used in the synthesis of the **ZnPc16-20@NCDs** assemblies were obtained from GO and ammonia. The results showed that the ZnPc photophysical/photochemical features were affected upon conjugation to CDs by π–π interactions, showing a decrease in the Φ_F of the Pcs, which was accompanied by an increase in the Φ_T. All conjugates were able to generate $^1O_2$ species, although with slightly less efficiency than the non-conjugated **ZnPc**, probably because the CDs screening effect limits the facile energy transfer from the triplet state to the dioxygen. The **ZnPc@NCDs** conjugates demonstrated PDT activity on the human breast cancer MCF-7 cell line upon irradiation, with the best obtained results for the **ZnPc19@NCDs** and **ZnPc20@NCDs** conjugates when compared with the corresponding non-immobilized **ZnPc**. At the highest conjugate concentration (100 µg/mL), it reached a cytotoxicity of approximately 50%.

Soon after, the authors reported the development and photodynamic efficiency towards MCF-7 cell lines of the novel hybrid materials **ZnPc21,22@NCDs** and **ZnPc21,22@biotin-NCDs** containing the neutral and cationic morpholine-substituted Pcs **ZnPc21** and **ZnPc22** and NCDs without or with tumour-targeting biomolecules such as biotin (**Figure 6**).[121] The access to neutral **ZnPc21** and cationic **ZnPc22** required the synthesis of the precursor 4-(2,5-dimethyl-4-(morpholinomethyl)phenoxy)phthalonitrile (**Pht4**) by the reaction of 2,5-dimethyl-4-(morpholinomethyl)-phenol hydrochloride monohydrate with the commercially available 4-nitrophthalonitrile followed by their tetramerization in the presence of Zn(OAc)$_2$, affording **ZnPc21**. The cationic **ZnPc22** was obtained by quaternization of the morpholino units in the presence of dimethylsulfate (DMS) or DMF (**Figure 6 A**). NCDs functionalized with biotin were prepared by reacting NCDs with biotin in the presence of the carboxyl-activating reagents *N,N′*-dicyclohexylcarbodiimide (DCC) and 4-dimethylaminopyridine (DMAP) in DMF.[121] The synthesis of the nanoplatforms required sonication followed by stirring (**Figure 6 B**).
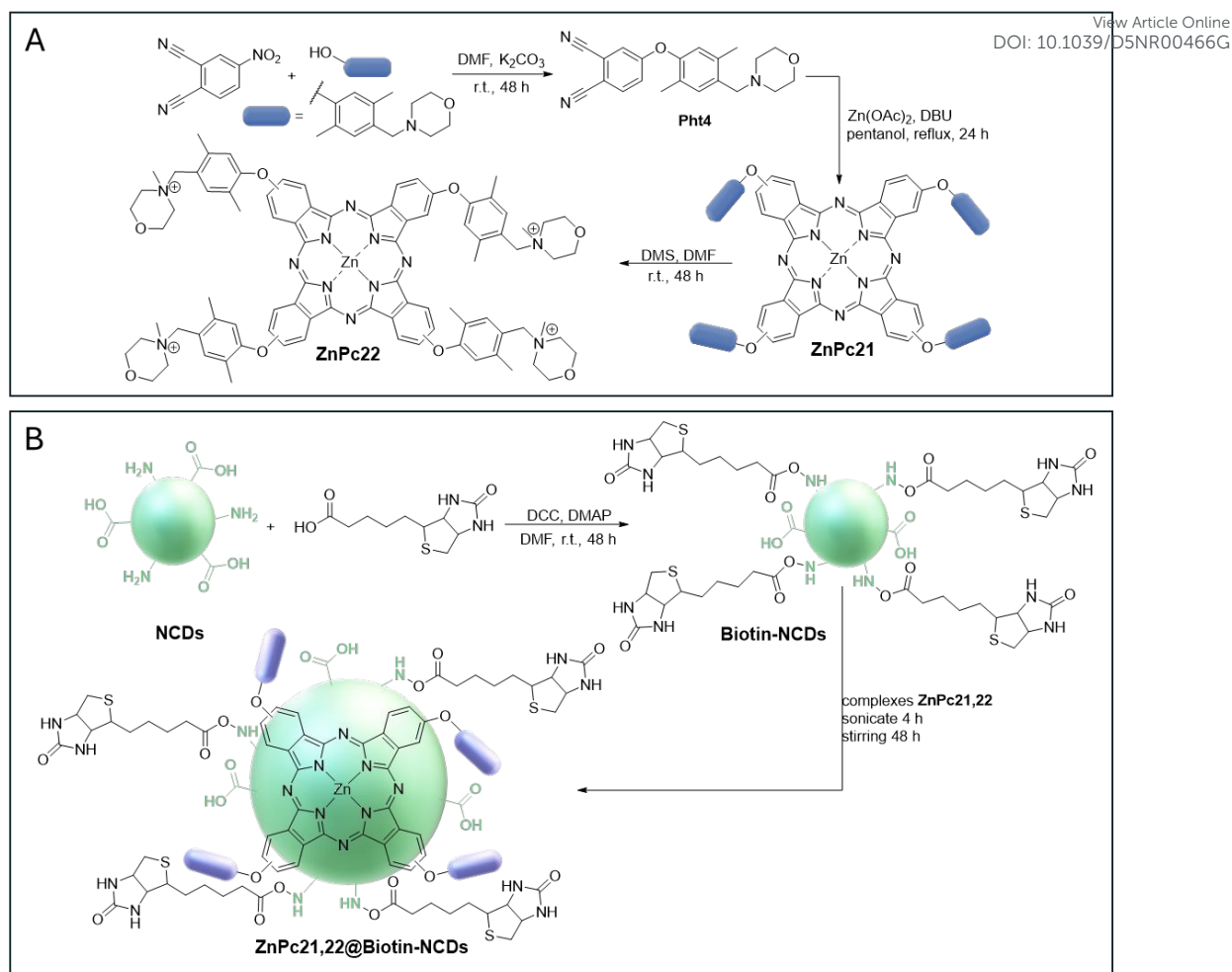
Figure 6. A Synthesis of **ZnPc21** and **ZnPc22**. **B** Synthesis of **biotin-NCDs** and **ZnPc21**, **22@biotin-NCDs** conjugates. [121]

The photophysical characterization of the **ZnPc21,22@NCDs** and **ZnPc21,22@biotin-NCDs** nanoassemblies showed that the conjugation caused a quenching of the emission, and also a dropped on the Φ_Δ values owing to screening effects. However, an increase in PDT activity was observed for the cationic dye in combination with biotin-functionalized NCDs. The PDT activity of the complexes (less cell viability) for **ZnPc21** and **ZnPc22** was higher than for their non-functionalized CDs conjugates. For **ZnPc21@CDs**, the low PDT activity may be related to its low Φ_Δ values when compared to the non-immobilized **ZnPc21** (**Table 2**). Indeed, cationic complexes generally perform better than non-charged complexes. This has previously been reported for Pcs[122] and other charged complexes in cancers,[123,124] where the net anionic membrane charge of cancer cells is believed to be susceptible to cationic drug complexes through electrostatic attraction. This may result in improved drug retention, and hence, more available Pcs for therapy. The combination of charge and biotin ligands improved the therapeutic efficacy of the complex.

Nanoscale Accepted Manuscript

In a related study, Nyokong *et al.*[125] reported the preparation of **ZnPc23@NCDs** and **ZnPc23@NSCDs** nanoassemblies by conjugating the cationic **ZnPc23** bearing morpholino moieties with **NCDs** and **NSCDs** (**Figure 7 A**). The NCDs and NSCDs were synthesized from citric acid under hydrothermal conditions (180 °C, 5 h) using urea and thiourea, respectively. The efficiency of the obtained assemblies was evaluated for the treatment of MCF7-cells under PDT, sonodynamic therapy (SDT), and combined PDT plus SDT (PSDT). Pc, CDs, and hybrids demonstrated cytotoxicity for PDT, SDT, and PSDT treatments in a concentration-dependent manner by cellular oxidative stress generated by the formation of ROS species (**Figure 7 B**). The determined IC_{50} values showed that Pc presented a relatively lower value than the conjugates for all three explored therapies. The results showed that $^1O_2$ was generated under all therapeutic conditions, and its presence increased upon conjugation. However, the generation of •OH radicals, which played a significant role in the eradication of cancer cells, only generated in the SDT and PSDT assays, showed a signal intensity decrease after the conjugation of Pc to the CDs (**Table 2**).
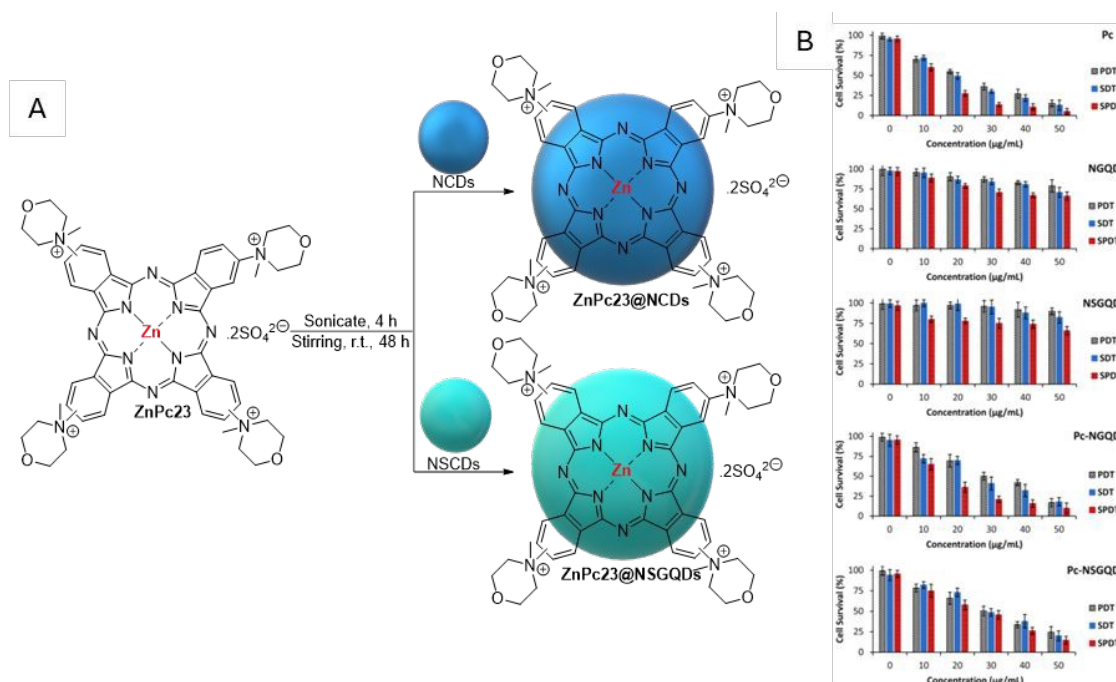

Figure 7. A Structure of the **ZnPc23@NCDs** and **ZnPc23@NSCDs** conjugates. **B** WST-assay post-PDT, SDT, and PSDT treatments at varied concentrations in water at 10 min irradiation time, n = 3. Parameters: PDT = irradiation dose of 170 J.cm⁻², power 2.3 W at 680 nm. SDT: frequency = 1 MHz, power = 1 W.cm⁻², 100% duty cycles. PSDT = combined PDT and SDT parameters with PDT applied first. Reproduced with permission. [125] Copyright 2021, Elsevier B.V.

Knowing that current PDT agents often suffer from low singlet oxygen quantum yields, photobleaching, and poor biocompatibility, Erdogmus¸ *et al.*[126–128] developed new hybrid nanomaterials to address these issues, based on the conjugation of indium(III) and zinc(II)

phthalocyanines with halogen and phenoxy substituents with GQDs obtained from citric acid and cysteine (GQDs@Cysteine) under hydrothermal conditions. Specifically, tetrakis(2-bromo-4-methylphenoxy)phthalocyaninato zinc(II), tetrakis(2-chloro-4-methylphenoxy)phthalocyaninato zinc(II), 4-tetrakis(2- chloro- 4-methylphenoxi)phtalocyaninat indium(III) chloride, and 4-tetrakis(2- bromo- 4-methylphenoxi)phtalocyaninato indium(III) chloride as regioisomeric mixtures were immobilized onto GQDs@cysteine through π–π stacking interactions. The photochemical and sonophotochemical properties of the resulting nanomaterials and their precursors were evaluated for potential applications in advanced cancer treatments with enhanced $^1O_2$. Briefly, all derivatives were exposed to light, sound, and a combination of both to measure their singlet oxygen production yield. The nanoconjugates of InPc and ZnPc exhibited improved Φ_Δ, compared to non-conjugated Pcs. In addition, it was observed that indium, being heavier than zinc, enhanced intersystem crossing and originated a higher singlet oxygen production yield (Table 2). These three studies confirmed that the sono-photodynamic approach (SPDT) enhances therapeutic efficacy by combining the advantages of light and ultrasound.

Table 2. Summary of the properties of non-covalently bonded **Pc@CDs** conjugates for cancer therapy and bioimaging.

CD type	Chemical conjugation	Phthalocyanine	Φ_{CD}	Φ_{Pc}	Φ_{Hybrid}	Application	Ref
CDs	Non-covalent (π-π stacking)	Zinc(II) phthalocyanine (**ZnPc**) 2,9(10),16(17),23(24)-Tetrakis[4-(N-methylpyridyloxy)]phthalocyanatozinc(II) (**ZnPc1**) 2,9(10),16(17),23(24)-Tetrakis(4-sulfonatophenyl)phthalocyaninatozinc(II) (**ZnPc14**)	**CDs** (0.11)[a]	* * * *	**ZnPc@CDs** (0.021)[a] **ZnPc1@CDs** (0.022)[a] **ZnPc14@CDs** (0.079)[a]	Determination of Φ_Δ values	[119]
NCDs	Non-covalent (π-π stacking)	2,9(10),16(17),23(24)-Tetrakis(2,6-di-tert-butyl-4-methylphenoxy)phthalocyaninatozinc(II) (**ZnPc16**)	**NCDs** (0.17)[a]	**ZnPc16** (0.16)[a] **ZnPc16** (0.78)[b] **ZnPc16** (0.50)[c]	**ZnPc16@NCDs** (0.09)[a] **ZnPc16@NCDs** (0.77)[b] **ZnPc16@NCDs** (0.30)[c]	PDT against MCF7 breast cancer cell	[119]
NCDs	Non-covalent (π-π stacking)	2,9(10),16(17),23(24)-Tetrakis(*tert*-butyl)phthalocyaninatozinc(II) (**ZnPc17**)	**NCDs** (0.17)[a]	**ZnPc17** (0.18)[a] **ZnPc17** (0.77)[b] **ZnPc17** (0.49)[c]	**ZnPc17@NCDs** (0.17)[a] **ZnPc17@NCDs** (0.83)[b] **ZnPc17@NCDs** (0.40)[c]	PDT against MCF7 breast cancer cell	[119]
NCDs	Non-covalent (π-π stacking)	2,9(10),16(17),23(24)-Tetrakis(phenylsulphanyl)phthalocyaninatozinc(II) (**ZnPc18**)	**NCDs** (0.17)[a]	**ZnPc18** (0.14)[a] **ZnPc18** (0.65)[b] **ZnPc18** (0.50)[c]	**ZnPc18@NCDs** (0.01)[a] **ZnPc18@NCDs** (0.67)[b] **ZnPc18@NCDs** (0.45)[c]	PDT against MCF7 breast cancer cell	[119]
NCDs	Non-covalent (π-π stacking)	2,9(10),16(17),23(24)-Tetrakis[(thiophenyl)benzo[*d*]thiazole]phthalocyaninatozinc(II) (**ZnPc19**)	**NCDs** (0.17)[a]	**ZnPc19** (0.18)[a] **ZnPc19** (0.67)[b] **ZnPc19** (0.54)[c]	**ZnPc19@NCDs** (0.11)[a] **ZnPc19@NCDs** (0.70)[b] **ZnPc19@NCDs** (0.50)[c]	PDT against MCF7 breast cancer cell line	[119]
NCDs	Non-covalent (π-π stacking)	2,9(10),16(17),23(24)-Tetrakis[(thiophenyl)benzo[*d*]thiazolium]phthalocyaninatozinc(II) Sulfate (**ZnPc20**)	**NCDs** (0.17)[a]	**ZnPc20** (0.10)[a] **ZnPc20** (0.75)[b] **ZnPc20** (0.35)[c]	**ZnPc20@NCDs** (0.09)[a] **ZnPc20@NCDs** (0.77)[b] **ZnPc20@NCDs** (0.30)[c]	PDT against MCF7 breast cancer cell	[119]

NCDs-biotin	Non-covalent (π-π stacking)	2,9(10),16(17),23(24)-Tetrakis[2,5-dimethyl-4-(methylmorpholino))-phenoxy]phthalocyaninatozinc(II) (**ZnPc21**)	**NCDs-biotin** (0.24)[a] **NCDs-biotin** (0.25)[d]	**ZnPc21** (0.20)[a] **ZnPc21** (0.68)[b] **ZnPc21** (0.67)[c]	**ZnPc21@NCDs-biotin** (0.16)[a] **ZnPc21@NCDs-biotin** (0.72)[b] **ZnPc21@NCDsbiotin** (0.47)[c]	PDT against MCF7 breast cancer cell	[121]
NCDs	Non-covalent (π-π stacking)	2,9(10),16(17),23(24)-Tetrakis[2,5-dimethyl-4-(methylmorpholin-4-ium))-phenoxy]phthalocyaninatozinc(II) Disulfate (**ZnPc22**)	**NCDs** (0.17)[a] **NCDs** (0.20)[d]	**ZnPc22** (0.20)[a] **ZnPc22** (0.69)[b] **ZnPc22** (0.53)[c] **ZnPc22** (0.14)[d] **ZnPc22** (0.11)[e]	**ZnPc22@NCDs** (0.15)[a] **ZnPc22@NCDs** (0.74)[b] **ZnPc22@NCDs** (0.58)[c] **ZnPc22@NCDs** (0.10)[d] **ZnPc22@NCDs** (0.08)[e]	PDT against MCF7 breast cancer cell	[121]
NCDs-biotin	Non-covalent (π-π stacking)	2,9(10),16(17),23(24)-Tetrakis[2,5-dimethyl-4-(methylmorpholin-4-ium))-phenoxy]phthalocyaninatozinc(II) Disulfate (**ZnPc22**)	**NCDs-biotin** (0.24)[a] **NCDs-biotin** (0.25)[d]	**ZnPc22** (0.20)[a] **ZnPc22** (0.69)[b] **ZnPc22** (0.53)[c] **ZnPc22** (0.14)[d] **ZnPc22** (0.11)[e]	**ZnPc22@NCDs-biotin** (0.14)[a]	PDT against MCF7 breast cancer cell	[121]
NCDs	Non-covalent (π-π stacking)	2,9(10),16(17),23(24)-Tetrakis(*N*-methyl-morpholin-4-ium)phthalocyaninatozinc(II) Disulfate (**ZnPc23**)	**NCDs** (0.70)[a]	**ZnPc23** (0.16)[a]	**ZnPc23@NCDs** (0.14)[a]	PSDT against MCF-7 breast cancer cell	[125]
SNCDs	Non-covalent (electrostatic interactions)		**SNCDs** (0.80)[a]	**ZnPc23** (0.16)[a]	**ZnPc23@SNCDs** (0.14)[a]		
GQDs@cysteine	Non-covalent (electrostatic interactions	4-tetra-(2-bromo-4-methylphenol) phtalocyaninatoindium(III) chloride	**GQDs@cysteine (0.41)[a]**	**InPcBr (0.02)[a] (0.75)[c] (0.96)[f]**	**InPcBr@ GQDs@cysteine (0.81)c (1.31)f**	Determination of Φ_Δ values using Sono-Photochemical methodologies	[126]

29

| GQDs@ cysteine | Non-covalent (electrostatic interactions) | tetrakis(2-bromo-4-methylphenoxy)phthalocyaninato zinc(II) tetrakis(2-chloro-4-methylphenoxy)phthalocyaninato zinc(II) | GQDs@ cysteine (0.41)a | ZnPcBr (0.20)a (0.63)c (0.94)f ZnPcCl [0.24)a (0.55)c (0.91)f | ZnPcBr@ GQDs@cysteine (0.68)c (0.95)f ZnPcCl@ GQDs@cysteine (0.57)c (0.93)f | Evaluation of the photocemical properties using sono-photodynamic procedures | [127] |
| GQDs@ cysteine | Non-covalent (electrostatic interactions) | 4-tetrakis(2- chloro- 4-methylphenoxi)phtalocyaninatoindium(III) chloride | GQDs@ cysteine (0.41)a | InPcCl (0.02)a (0.65)c (0.94)f | InPcCl@ GQDs@cysteine (0.79)c (1.17)f | Assessment of Singlet oxygen yield Φ_Δ using ultrasound and light | [128] |

[a]Φ_f, [b]Φ_T, [c]Φ_Δ in DMSO; and [d]Φ_f, [e]Φ_Δ in H_2O and [f]Φ_Δ in DMSO using ultrasound at 35 kHz and light exposition at 7.05 x 10^{15} photon $s^{-1}cm^{-2}$.

2.1.3.2. Antibacterial applications

The conjugation of the CDs and Pcs was also explored for antibacterial applications (**Table 3**), considering previous reports that showed improvements in the required photophysicochemical features after the formation of the hybrids. Nyokong *et al*. conducted the first study in the context of aPDT using **MPc24@CDs** nanoassemblies (M = 2H, Zn, or In) against the multidrug-resistant *Staphylococcus* (**Figure 8**).[129] The photoactive platforms were prepared from the free-base **H₂Pc24** with acetylphenoxy units and the corresponding **ZnPc24** and **InPc24** complexes (**Figure 8 A**); in the selection of these Pcs the authors had in account the antibacterial features associated with reactive carbonyl group.[130,131] The synthetic strategy involved the reaction of 4-hydroxyacetophenone with 4-nitrophthalonitrile to afford the required phthalonitrile **Pht5**, followed by its tetramerization in DMAE and DBU with LiCl or $ZnCl_2$ to obtain **H₂Pc24** or **ZnPc24**, respectively (**Figure 8 A**).[129] **InPc14** was obtained by the reaction of **H₂Pc24** with anhydrous InCl in dry DMF and DBU. The results showed that the efficiency of the conjugates to produce $^1O_2$ parallels that observed by the non-conjugated Pcs being the most efficient the indium complex, followed by the zinc complex, and then the free-base (values ranging from Φ_Δ = 0.20 to 0.79 DMSO). The aPDT activity of both phthalocyanines and nanoconjugates was tested against multidrug-resistant *Staphylococcus aureus* (*S. aureus*), where **InPc24@CDs** was highly effective causing a 9.68 log reduction in the bacterial viability at 10 μM (based on Pc) when compared to 3.77 log reduction of **ZnPc24@CDs** (**Figure 8 C** and **D**).
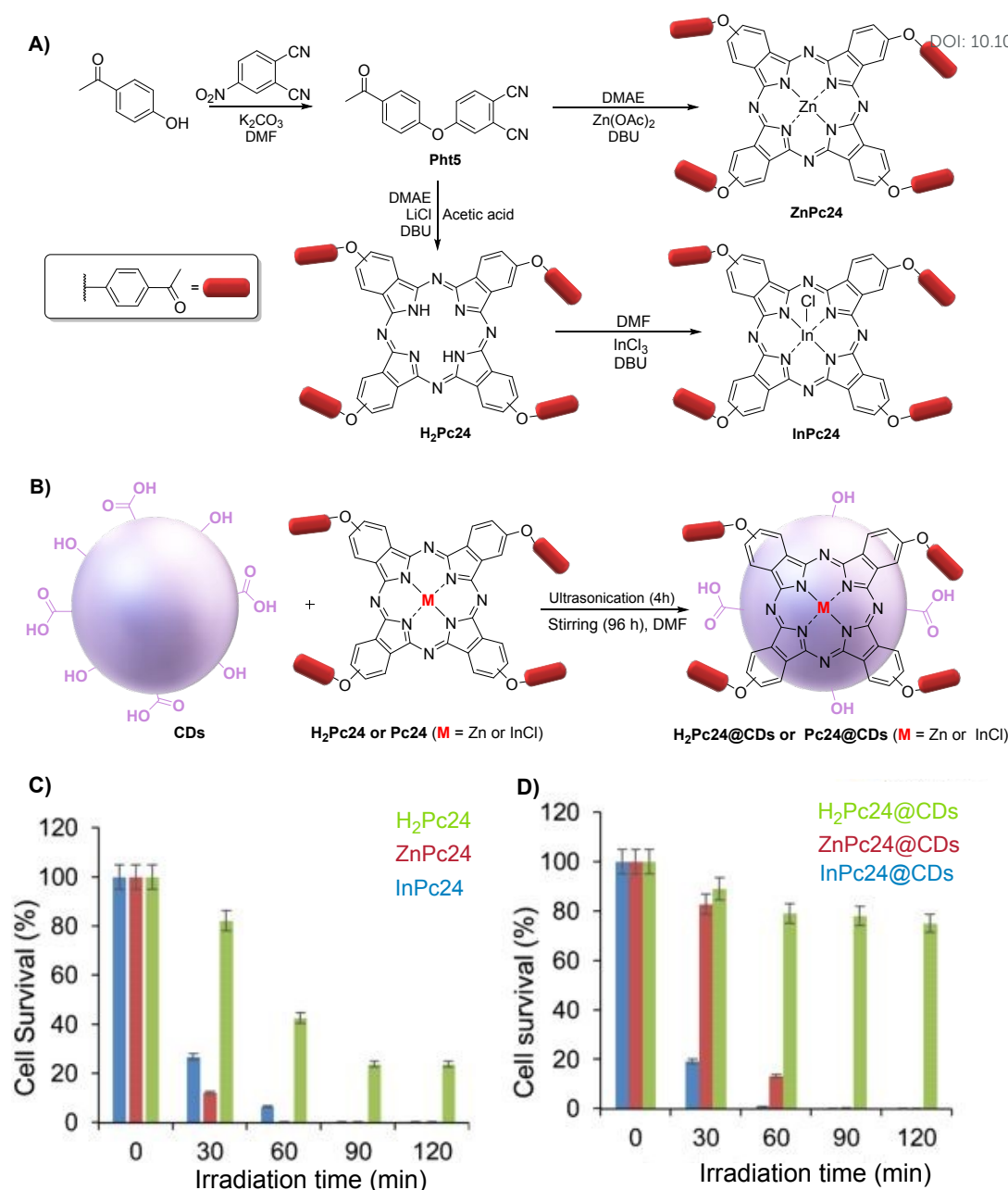
Nanoscale Accepted Manuscript

Figure 8. A Synthesis of **H₂Pc24**, **ZnPc24**, and **InPc24** and **B** conjugation of Pcs with CDs. **C** Survival graphs of *S. aureus* incubated with 10 µM of photosensitizer for Pcs alone and for the conjugates **D** with irradiation at 670 nm. Reproduced with permission.[129] Copyright 2019, Elsevier B.V.

Photodynamic action of **ZnPc25@NCDs** nanoassemblies, obtained from nitrogen-doped CDs (**NCDs**) and **ZnPc25** bearing benzoimidazolylphenoxy units, was evaluated towards gram-positive bacteria S*. aureus*.[132] The hybrid constituents were obtained following well-established approaches, and the photophysical/photochemical characterization showed improved singlet oxygen ($\Phi_\Delta = 0.45$) and triplet state quantum yields ($\Phi_T = 0.60$) compared to the non-immobilized **ZnPc25** ($\Phi_\Delta = 0.36$ and $\Phi_T = 0.54$). In the antibacterial tests under UV light exposure, the **ZnPc25@NCDs** hybrid achieved a 99.9% bacterial kill rate, outperforming free **ZnPc25** (99.86%). This aligns with its higher singlet oxygen production. In 2024, Özçesmeci et al. reported the

synthesis of new nanoconjugates through the non-covalent conjugation of a copper(II) phthalocyanine, substituted with 2,3-dihydroxypropoxy groups in the non-peripheral positions, to carbon dots (**CDs**) and carbon-boron quantum dots (**CBDs**). The antimicrobial photodynamic therapy (aPDT) efficacy of each hybrid was evaluated against Gram-positive bacteria (*E. hirae* and *E. faecalis*), Gram-negative bacteria (*E. coli, P. aeruginosa*, and *B. subtilis*), and microfungi (*C. parapsilosis* and *C. albicans*). The selected phthalocyanine was obtained by deprotecting the 2,2-dimethyl-1,3-dioxolan-4-yl)methoxy groups in 1,8(11),15(18),22(25)-tetrakis[(2,2-dimethyl-1,3-dioxolan-4-yl)methoxy]phthalocyaninatocopper(II) using acetic acid. The **CBDs** were synthesized via microwave-assisted synthesis, involving citric and boric acids. The aPDT evaluation revealed the lowest minimum inhibitory concentration (MIC) of 4 mg/L against Gram-positive bacteria, which decreased further post-irradiation, significantly enhancing antimicrobial effects. Additionally, the study demonstrated promising biological applications for the new conjugates like radical scavenging activity, antidiabetic effects, and DNA cleavage activity, inhibition of biofilm formation by *S. aureus* and *P. aeruginosa*.

Nanoscale Accepted Manuscript

Table 3. Summary of the properties of non-covalently bonded **Pc@CDs** conjugates for antibacterial activity.

CD type	Chemical conjugation	Phthalocyanine	Φ_{CD}	Φ_{Pc}	Φ_{Hybrid}	Application	Ref
CDs	Non-covalent (π-π stacking)	2,9(10),16(17),23(24)-Tetrakis[(phenoxy)ethan-1-one)]phthalocyanine (**H₂Pc24**)	**CDs** (0.35)[a]	**H₂Pc24** (0.20)[a] **H₂Pc24** (0.31)[b] **H₂Pc24** (0.22)[c]	**H₂Pc24@CDs** (0.0.39)[a] **H₂Pc24@CDs** (0.27)[b] **H₂Pc24@CDs** (0.20)[c]	PDT against *S. aureus*	[129]
CDs	Non-covalent (π-π stacking)	2,9(10),16(17),23(24)-Tetrakis[(phenoxy)ethan-1-one)]phthalocyaninatozinc(II) (**ZnPc24**)	**CDs** (0.35)[a]	**ZnPc24** (0.13)[a] **ZnPc24** (0.78)[b] **ZnPc24** (0.72)[c]	**ZnPc24@CDs** (0.059)[a] **ZnPc24@CDs** (0.85)[b] **ZnPc24@CDs** (0.77)[c]	PDT against *S. aureus*	[129]
CDs	Non-covalent (π-π stacking)	2,9(10),16(17),23(24)-Tetrakis[(phenoxy)ethan-1-one)]phthalocyaninatoindium(III)chloride (**InPc24**)	**CDs** (0.35)[a]	**InPc24** (0.046)[a] **InPc4** (0.84)[b] **InPc4** (0.75)[c]	**InPc24@CDs** (0.054)[a] **InPc24@CDs** (0.90)[b] **InPc24@CDs** (0.79)[c]	PDT against *S. aureus*	[129]
NCDs	Non-covalent (π-π stacking)	2,9(10),16(17),23(24)-Tetrakis [4-(4-(5-chloro-1H-benzo[d]imidazol-2-yl)phenoxy]phthalocyaninatozinc(II) (**ZnPc25**)	**NCDs** (0.19)[d]	**ZnPc25** (0.17)[a]	**ZnPc25@NCDs** (0.12)[a]	PDT against *S. aureus*	[132]
CBDs	Non-covalent (π-π stacking)	1, 8(11), 15(18), 22(25)-tetrakis [(2,2-dimethyl-1,3-dioxolan-4-yl)methoxy]phthalocyaninato copper (II)	-	-	-	PDT against Gram-positive bacteria (E. hirae and E. faecalis), Gram-negative bacteria (E. coli, P. aeruginosa and B. subtilis),	[133]

[a]Φ_f, [b]Φ_T, [c]Φ_Δ in DMSO; and [d]Φ_f in H₂O.

2.1.4. Photocatalytic applications

The potential of Pc@CDs to generate ROS is much lower in the context of photocatalytic applications than for phototherapeutic ones. However, some promising outcomes were achieved when the photooxidation of 4-chlorophenol was evaluated in the presence of unsymmetric polystyrene membranes **ZnPc@NCDs-PS-membrane** bearing nanoassemblies consisting of non-substituted **ZnPc** and **CDs** with amino substituents (**NCDs**) covalently linked through an amide bond to carboxylated polystyrene (**CO₂H-PS**).[134] The synthetic strategy involved first the non-covalent conjugation of the unsubstituted **ZnPc** to the **NCDs,** obtained from the carbonization of citric acid and polyethyleneimine, according to previous works in the literature.[100,135] Subsequently, before membrane casting, the resulting **ZnPc@NCDs** hybrid was covalently linked to **CO₂H-PS** *via* an amide bond using thionyl chloride to mediate the formation of activated acyl chloride functionalities. This step was considered to avoid the leaching of ZnPc from the membrane, as observed when **ZnPc** or **ZnPc@NCDs** were simply mixed with the polymer solution (without prior conjugation). Then, the **ZnPc@NCDs-PS-membrane** was obtained by casting on glass slides a dispersion in DMF of non-functionalized polystyrene (PS) plus the conjugate, followed by precipitation in a methanol bath.[134] The photophysical characterization confirmed the ability of the membranes to generate $^1O_2$ in ethanol (Φ_Δ = 0.43) and water (Φ_Δ = 0.37) *versus* **ZnPc@NCDs** (Φ_Δ = 0.49), allowing to perform the photocatalytic oxidation of 4-chlorophenol in aqueous media. The study showed that the reaction followed second-order kinetic at 3.24×10^{-4} mol L^{-1} with a k_{obs} of 35.9 L mol^{-1} min^{-1} and a half-life of 86 min. Although the membrane was able to photodegrade 4-chlorophenol in water, its efficiency was not fully revealed.

A recent study explored combination of CDs functionalized with **NiPc** with Cu–In–Zn–S quantum dots (**CIZS QDs**) for surface proton generation and reduction. The synthesis of the ternary **CIZS QDs/NiPc@CDs** composite is presented in **Figure 9 A**. [136] The size of the CIZS QDs and CDs was determined by transmission electron microscopy (TEM), corresponding to 3.5 ± 0.5 and 2.5 ± 0.5 nm, respectively (**Figure 9 B** and **C**). The nanocomposite **CIZS QDs/NiPc@CDs** revealed the formation of smaller **NiPc@CDs** and larger **CIZS QDs**. The HRTEM analysis of the **CIZSQDs/NiPc@CDs** confirms the presence of both individual nanostructures by the existence of lattice spacings of 0.310 nm, corresponding to the **CIZS QDs**, and 0.210 nm, corresponding to the CDs (**Figure 9 D** and **E**). Elemental mapping images of the **CIZS QDs/NiPc@CDs** further confirmed that the presence of In, Cu, Zn, S, Ni, and C were well merged, indicating that **CIZS QDs** and **NiPc@CDs** were well integrated to form the nanocomposite material (**Figure 9 F-J**). The developed ternary nanocomposite **CIZS QDs/NiPc@CDs** were tested in terms of their performance in photocatalytic hydrogen evolution coupled with organic oxidation electron/hole extraction. A preliminary study, based on the photocatalytic degradation of rhodamine B (RhB), showed (**Figure 9 K**) that the **CIZS QDs/NiPc@CDs** nanocomposite presented higher photodegradation activity. The authors demonstrated

that the dominant mechanism was based on photogenerated holes because with the addition of ethylenediaminetetraacetic acid (hole quencher), the photodegradation reaction was completely inhibited (**Figure 9 I**). This clearly illustrates that the photogenerated holes mainly contribute to the degradation of RhB in the **CIZS QDs/NiPc@CDs** composite photocatalyst system, which also proves the effectiveness of the hole-extraction strategy by **NiPc@CDs** modification. The performance of the **CIZS/NiPc@CDs** nanocomposite was further assessed for the photocatalytic hydrogen evolution coupled with the oxidation of different alcohols. **CIZS QDs/NiPc@CDs** photocatalytic hydrogen production via MeOH oxidation, revealed the highest rate among all the tested nanomaterials, reaching 1.121 mmol g^{-1} h^{-1} (**Figure 9 M** and **N**). Moreover, the oxidation of biomass-derived furfuryl alcohol (FFA) generated an hydrogen production that reached 2.516 mmol g^{-1} h^{-1} (**Figure 9 O** and **P**).
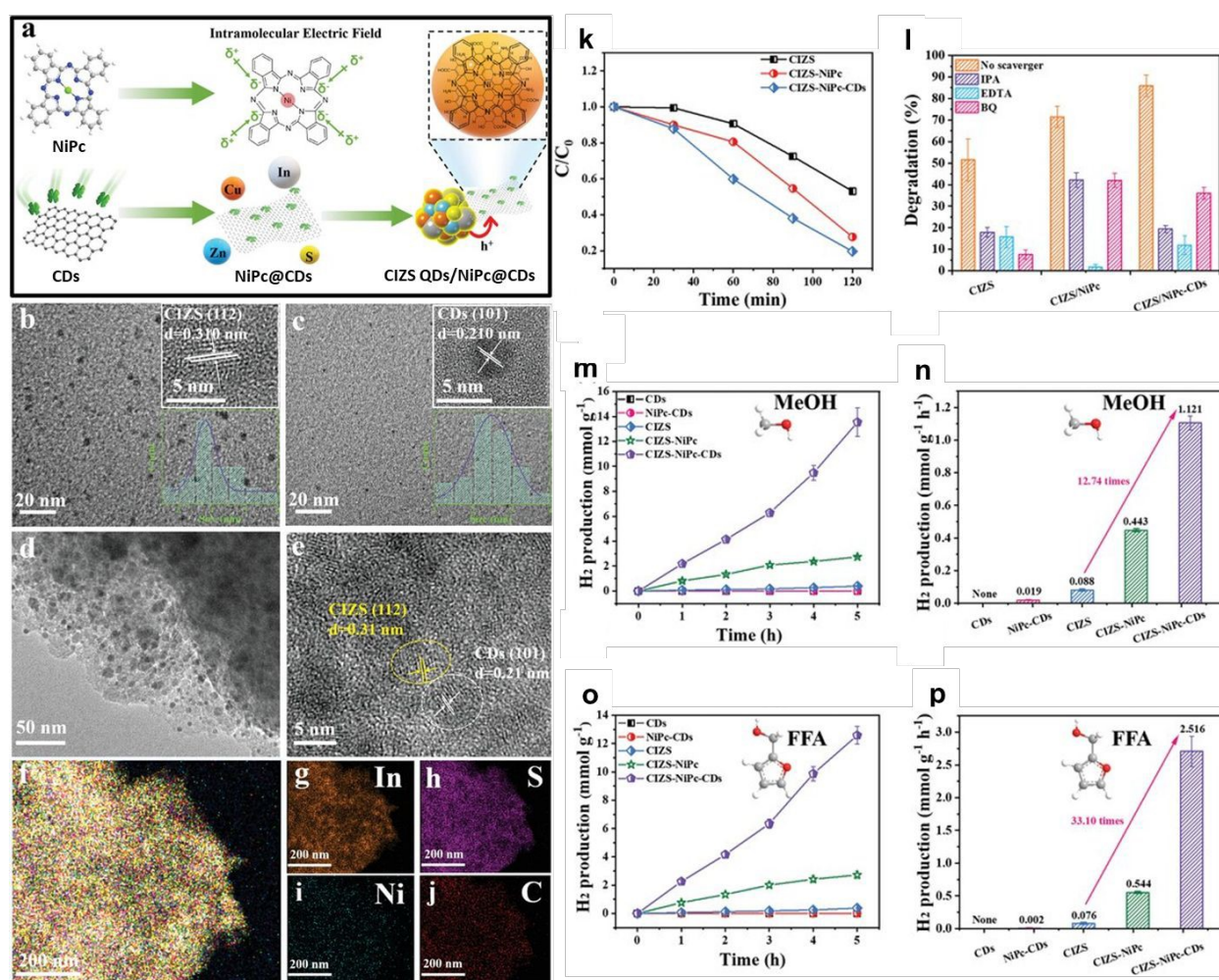

Figure 9. **A** Schematic diagram for the construction of the ternary **CIZS QDs/NiPc@CDs** composite. **B** TEM images of **CIZS QDs** and **C CDs** and the corresponding HRTEM images (top insets) and size distribution histograms (bottom insets) obtained by counting 100 particles. **D** TEM and **E** HRTEM images of **CIZS QDs/NiPc@CDs**. **F–J** The corresponding elemental mapping images of **CIZS QDs/NiPc@CDs**. **K** Photocatalytic degradation ratio of RhB over **CIZS QDs**, **CIZS QDs/NiPc**, and **CIZS QDs/NiPc@CDs** under

visible-light irradiation. **I** Active species trapping experiment during photocatalytic degradation of RhB over **CIZS QDs/NiPc@CDs** with the addition of quenchers of h⁺ (EDTA), •O²⁻ (BQ), and •OH (isopropanol, IPA). Photocatalytic hydrogen evolution performance over **CDs**, **NiPc@CDs**, **CIZS QDs**, **CIZS QDs/NiPc**, and **CIZS QDs/NiPc@CDs** coupled with (**M**), (**N**) methanol oxidation and (**O**, **P**) FFA oxidation reactions. Reproduced with permission.[136] Copyright 2023, John Wiley & Sons, Inc.

2.1.5. Miscellaneous applications

With future applications in molecular sensors and solar cells in mind, Majeed *et al*. studied the nonlinear optical responses of carbazole-substituted ZnPc (**ZnPc26A-C**) conjugated to CDs and in thin films (TF) of polystyrene (PS) (**Figure 10**).[137] These **ZnPcs** were obtained by tetramerization of the suitable phthalonitriles in quinolone at 80 ºC in the presence of anhydrous Zn(OAc)$_2$ and DBU. **Phts 6A-C** were prepared from the reaction of commercially available 4,5-dichlorophthalonitrile with the required carbazoles in dry DMF in the presence of cesium fluoride.
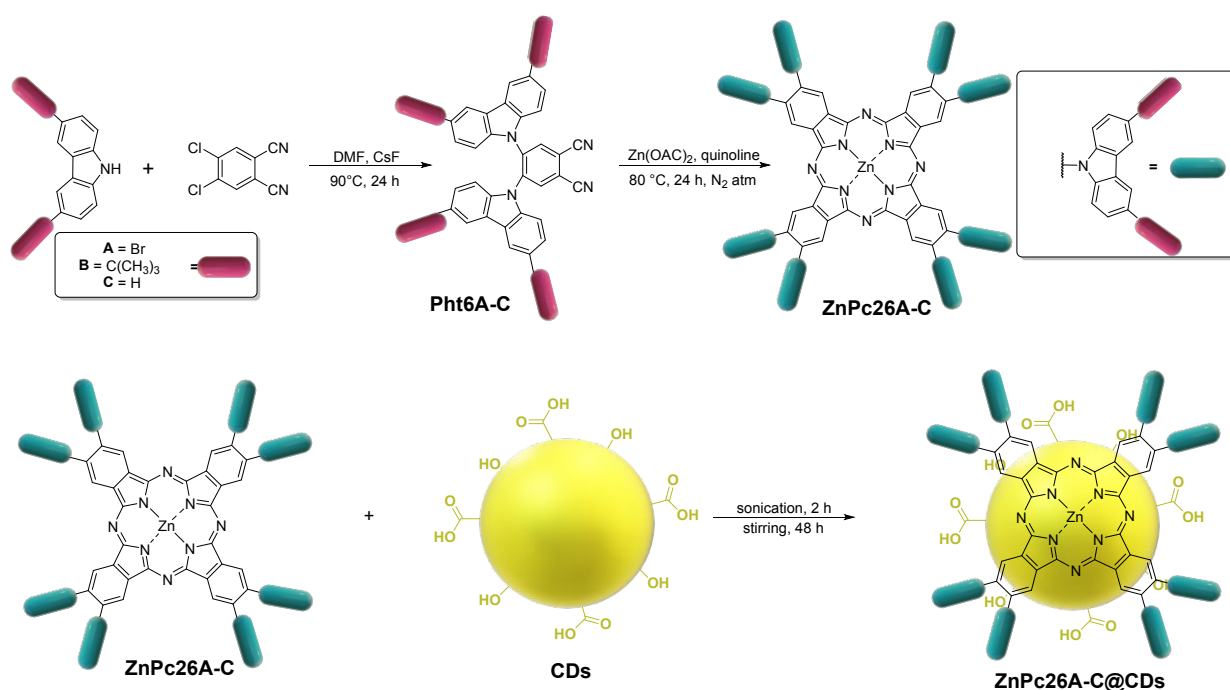

Figure 10. Preparation of **ZnPc26A-C** substituted with eight carbazole units used in the synthesis of the nanoassemblies **ZnPc26A-C@CDs** further immobilized in polystyrene films. [137]

The immobilization of the ZnPc in CDs obtained from the pyrolysis of citric acid in the presence of NaOH afforded the required nanoassemblies **ZnPc26A-C@CDs** that after being embedded in PS films showed an average thickness of 0.45–0.62 mm. These thin films of **ZnPc26A-C@CDs-PS** showed promising optical limiting parameters in different solvents, with improved optical limiting performance, characterized by increased third-order susceptibilities and hyperpolarizabilities, as well as lower limiting threshold values.

In 2021, AlMarzouq *et al*. selected the analogue manganese phthalocyanine with eight carbazole units (**MnPc26C**) to conjugate with CDs which were obtained through pyrolysis of calcium acetate at 200 °C, to evaluate the influence of the carbazole substituents and CDs on the redox mechanism of MnPc.[138] The electrochemical performance of **MnPc26C** and of the resulting conjugate was investigated using cyclic voltammetry (CV), square wave voltammetry (SWV), and spectroelectrochemistry (SEC), showing extended metal-based redox processes at low potentials. Furthermore, the carbazole substituents provided additional redox activity facilitating the electropolymerization of the complex onto the electrode surface, simplifying the electrode modification.

2.2. Covalent functionalization

2.2.1. Fundamental insights into Pc@CDs features

The covalent functionalization of the CDs with Pcs has been significantly less explored compared to the non-covalent approach. However, some different applications can be already found in the literature and are summarized on the **Table 4**. One of the most relevant advantages of exploring the covalent bond is the stability of the conjugate. The most common approaches for stablishing stable covalent bonds between CDs and Pcs generally involve esterification or amidation reactions. In 2020, Prato *et al*. developed the **ZnPc27@NCDs** hybrid by linking the amorphous NCDs to the non-symmetric **ZnPc27** via an amide bond (**Figure 11 A**);[139] This dye acted as an electron donor with a large extended π-surface and strong absorption in the visible spectrum. Intermolecular interactions were confirmed by steady-state and pump-probe transient absorption spectroscopy, which revealed symmetry-breaking charge transfer/separation and recombination dynamics within pairs of Pcs. Moreover, steady-state fluorescence experiments showed quenching in the formed hybrid material, accompanied by a red shift of the fluorescence maximum, upon excitation at λ = 387 nm (**Figure 11 A**). The CDs simplify the electronic interactions between the studied Pcs, suggesting that they can be used to support electronic couplings in multichromophoric arrays, which can increase their application in organic electronics, photonics, and/or artificial photosynthesis systems. Examples of this type of conjugation and their respective potential applications are discussed in the following sections.
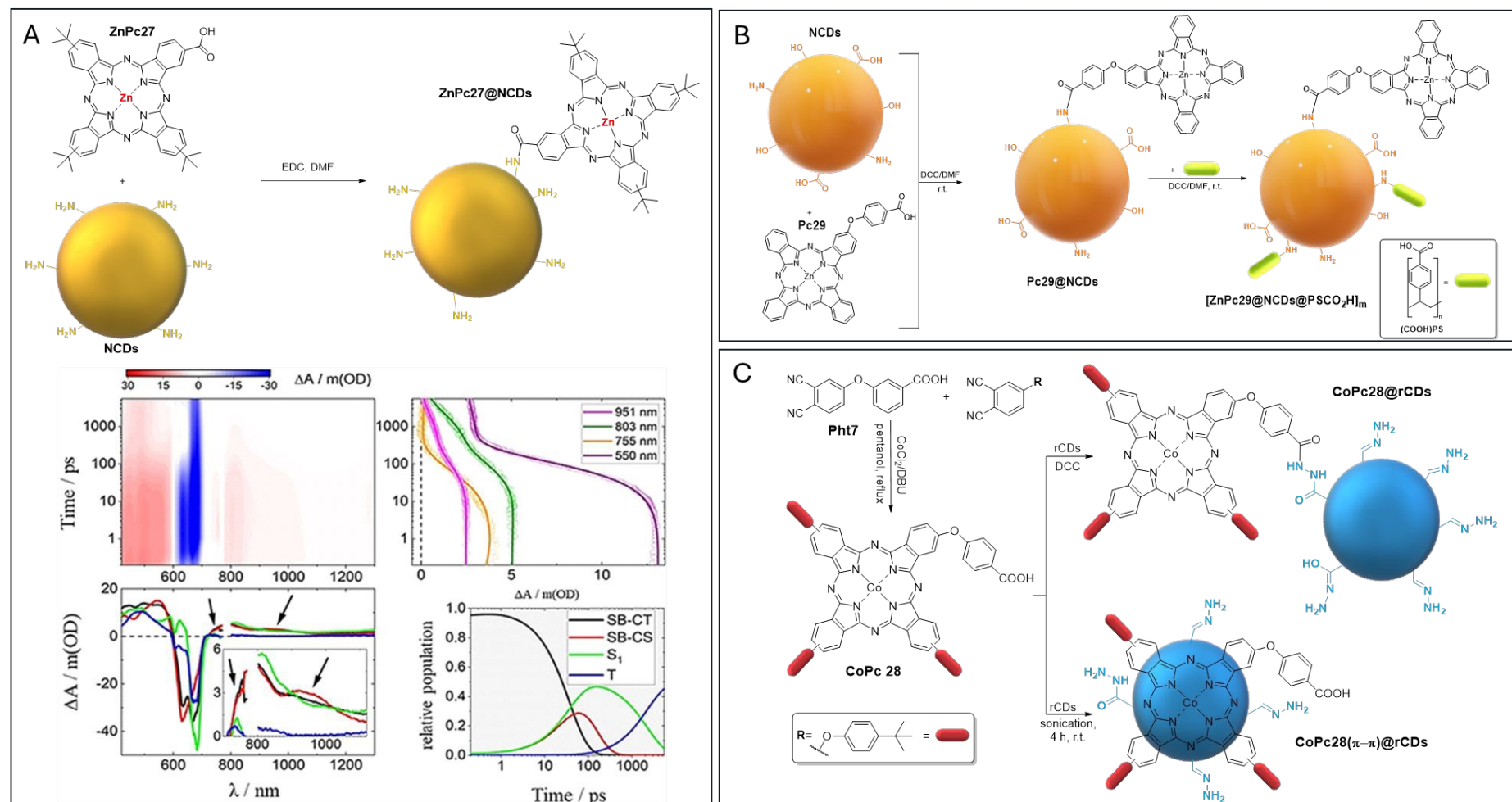
Figure 11. A NCDs covalently linked to **ZnPc27**: (**1**) Differential absorption 3D map obtained by fsTAS of **ZnPc27@NCDs** in CH$_3$OH at room temperature upon excitation at λ = 387 nm (**2**)Time absorption profiles and corresponding line fittings at λ = 951 (magenta), 803 (dark green), 755 (orange), and 550 nm (purple) (**3**) Species-associated differential spectra of SB-CT (black), SB-CS (red), S1 (green), and T1 (blue) excited states (**4**)concentration evolution over time.[139] **B** Synthesis of **CoPc28** and their functionalization with **rCDs** to obtain **CoPc28@rCDs** and **CoP28(π-π)@rCDs** hybrids.[140] **C** Strategy used in the preparation of **[ZnPc29@NCDs@PSCO$_2$H]$_m$** membrane.[141]

2.2.2.   Electrocatalytic applications

The possibility of using CDs in the oxygen reduction reaction (ORR) merits special attention from the scientific community because of their efficiency in lowering the oxygen adsorption and first electron transfer barriers and consequently providing enhanced electrocatalytic activity.[142] This reaction plays an important role in fuel cells and metal-air batteries, and although Pt-based nanomaterials display excellent activities for ORR, their high cost and poor durability limit their wide application. Thus, CDs can be an excellent alternative, although some drawbacks, such as low limiting current density and potential onset, still require improvement. Based on the knowledge that the hybridization of CDs with other functional materials is a potential strategy for improving their ORR catalytic properties prompted Koh *et al.* in 2017 to evaluate the ORR electrocatalytic activity of **FePc@CDs** conjugates obtained through the coordination of the metal ion in **FePc** to the CDs.[143] In the selection of **FePc**, the authors considered its efficiency as an electrocatalyst for the ORR. The CDs were obtained by hydrothermal treatment of GO using NH_4OH and H_2O_2. The immobilization of FePc on the CDs was performed at room temperature in DMSO and pyridine, and the color change from blue to green confirmed the successful coordination of the metal to the CDs. The results from the electrochemical assays showed a higher performance of **FePc@CDs** when compared with CDs, and a Pt/C electrode was selected for comparison. All samples in O_2-saturated electrolyte exhibited cathodic current peaks contrary to the assays performed in N_2 that exhibited only very weak cathodic current peaks due to intrinsic redox.[144] The positive shift of the ORR peak of **FePc@CDs** (0.1 V *vs*. Hg/HgO) when compared with the CDs peak (0.18 V *vs*. Hg/HgO) and the two times higher oxygen reduction current of the conjugate was justified to be mainly due to the charge transfer behaviour from CDs to electronegative **FePc**. The results showed that **FePc@CDs,** like the Pt/C electrode, mediated the desired four-electron reaction in an alkaline electrolyte, contrary to CDs, which presented a two-electron transfer process yielding HO_2^-. Other positive outcomes compared to Pt/C are a higher limiting current density, excellent methanol tolerance, insensitivity to CO poisoning, and electrochemical stability. Thus, **FePc@CDs** have the potential to be used as efficient nonprecious electrocatalysts for the ORR and may be used in commercial applications of fuel cells.

Knowing that the elimination of the oxygen content on the surface of CDs is responsible for reducing the energy band gap of the reduced carbon dots **rCDs** compared to amino-functionalized CDs **NCDs**, resulting in materials with improved electron transfer processes and conductivity, Centane *et al.*[141] developed conjugates based on the **CoPc28** (**Figure 11 B**) covalently linked to **NCDs** and **rCDs** and evaluated their performance during the electrocatalysis of hydrazine on a glassy carbon electrode (GCE). For comparison, the authors also considered the development of analogues nanoassemblies obtained just from π–π interactions. Unsymmetrical **CoPc28** was obtained by the condensation of 4-(*p-tert*-butylphenoxy)phthalonitrile (**Pht7**) and 4-(4-carboxy-phenoxy)phthalonitrile) in pentanol at 160 °C and in

Nanoscale Accepted Manuscript

the presence of $CoCl_2.6H_2O$ and DBU (**CoPc28**, **Figure 11 B**). [140] NCDs were synthesized by oxidative cutting of GO sheets with $KMnO_4$ and H_2SO_4, followed by the reaction of the obtained CDs with an ammonia solution in the presence of EDC/*N*-hydroxysuccinimide (NHS). On the other hand, rCDs were obtained by treating the CDs in water with hydrazine hydrate to eliminate the high number of oxygen-containing functionalities. The **CoPc28@rCDs** and **CoPc28@NCDs** hybrids were obtained by reacting **CoPc28** and the required CDs in DMF and using EDC/NHS as activating carboxyl reagents. The analogues π-π hybrids (**CoP28(π-π)@rCDs** and **CoPc28(π-π)@NCDs**) were obtained by sonication of the required constituents. The efficiencies of the precursors and conjugates covalently and non-covalently linked in the electrocatalysis of hydrazine were evaluated using a GCE. The procedure was conducted by placing each hybrid on the GCE, followed by drying at 70 °C to obtain the following electrodes: **CoPc28@GCE/rCDs**, **CoPc28@GCE/NCDs**, **CoPc28(π-π)@GCE/rCDs**, and **CoPc28(π-π)GCE/NCDs**. The **rCDs@GCE**, **NCDs@GCE**, and **CoPc@GCE** electrodes were prepared by the same procedure. Low LOD values for hydrazine oxidation were obtained in the presence of the electrodes that containing the hybrids prepared by covalent conjugation **CoPc28@GCE/rCDs** and **CoPc28@GCE/NCDs**. It was also observed that the hybrids composed by the rCDs gave better LOD values than the corresponding NCDs hybrids. The results obtained confirmed that the elimination of excessive oxygen-containing groups on the surface of the CDs does indeed tune the energy band gap, improving the required electron transfer and conductivity.

To compare how the efficiency of a Pc to generate $^1O_2$ was affected by the type of bond linked to the CDs, Nyokong *et al.* (2019) developed polystyrene membranes **[ZnPc29@NCDs@PSCO$_2$H]$_m$** bearing **NCDs** covalently linked to the unsymmetrical **ZnPc29** bearing a carboxyphenoxy unit and to carboxyl-functionalized polystyrene (PSCO$_2$H) through amide bonds; membranes resulting of the π–π interactions between the **ZnPc29** and the **NCDs@PSCO$_2$H** were also prepared, **[πZnPc29@NCDs@PSCO$_2$H]$_m$** (**Figure 11 C**). [141] The NCDs were obtained through the hydrothermal treatment of GO with ammonia and during the covalent conjugation process their coupling with **ZnPc29** and then to PSCO$_2$H was performed in DMF in the presence of DCC. The observation of shifts in the region of the amide peak in the FTIR spectra, from 1667 cm^{-1} in **ZnPc29@NCDs** to 1657 cm^{-1} in **ZnPc29@NCDs-(COOH)-PS**, suggested successful conjugation. Initially, the NCDs were monodispersed with a size of approximately 14 nm, but after conjugate formation, the size increased to 21 nm. The XRD diffractograms showed that the synthesized nanoconjugates were amorphous, like their constituents. Photophysical/photochemical characterization revealed that the hybrid materials exhibited better performance prior to incorporation into the membranes (e.g., Φ_Δ of 0.33 (π) and 0.44 (c) compared to 0.16 (π) and 0.29 (c) after incorporation). Moreover, hybrids with covalent linkages consistently outperformed those with π-π interactions in both conditions.

2.2.3. Sensing applications

In 2022, Mashazi *et al.* developed an electrochemical sensor for the detection of catecholamine neurotransmitters using composites of **CoPc30** and aminated CDs (NCDs), covalently functionalized onto an isophthalic acid electrografted gold electrode (Au-IPA).[145] The electrochemical performance of the composite-modified gold surface was evaluated using CV, differential pulse voltammetry (DPV), SWV, and electrochemical impedance spectroscopy (EIS) in PBS and in newborn calf serum (NCS). The sensor demonstrated improved electrochemical performance for detecting dopamine (DA), epinephrine (EP), and norepinephrine (NR), with broad linear ranges (1.0–50 µM in PBS and 0.0–60 µM in serum) and low detection limits in the µM range. Moreover, the engineered electrochemical sensor exhibited an interesting capability to suppress background current and was effectively used for the detection of catecholamine neurotransmitters in newborn calf serum with high recovery.

Nanoscale

Table 4. Summary of the properties and applications of covalently bonded **Pc@CDs** conjugates.

CD type	Chemical conjugation	Phthalocyanine	Φ_{CD}	Φ_{Pc}	Φ_{Hybrid}	Application	Ref.
NCDs	Covalent	9(10),16(17),23(24)-Tri-*tert*-butyl-2-carboxy-5,28:14,19-diimino-7,12:21,26-dinitrilotetrabenzo[*c,h,m,r*][1,6,11,16]tetraazacycloeicosinato-(2⁻)-$N^{29},N^{30},N^{31},N^{32}$ zinc(II) (**ZnPc27**)	NCDs (0.17)[a]	ZnPc 27 (0.15)[a]	*	Charge tranfer	[139]
CDs, rCDs and NCDs	Covalent and/or non-covalent (π-π stacking)	2-Mono[(4-carboxyphenoxy)]-9(10),16(17),23(24)-Tris[*tert*-butylphenoxy)]phthalocyaninatocobalt(II) (**CoPc28**)	*	*	*	Electrooxidation of hydrazine	[141]
NCDs	Covalent and/or non-covalent (π-π stacking)	2-Mono[(4-carboxyphenoxy)]-9(10),16(17),23(24)-Tris[phenyl)]phthalocyaninatozinc(II) (**ZnPc29**)	NCDs (0.16)[a]	ZnPc29 (0.16)[a] ZnPc29 (0.70)[b] ZnPc29 (0.56)[c]	πZnPc29@NCDs (0.18)[a] πZnPc29@NCDs (0.70)[b] πZnPc29@NCDs (0.33)[c] ZnPc29@NCDs (0.19)[a] ZnPc29@NCDs (0.49)[b] ZnPc29@NCDs (0.44)[c]	Determination of Φ_Δ values	[140]
NCDs	Covalent	2,9(10),16(17),23(24)-Tetrakis[(3-carboxyphenoxy)]phthalocyaninatocobalt(II) (**CoPc30**)	*	*	*	Electrochemical sensors for dopamine, norepinephrine, and epinephrine detection	[145]

[a]Φ_f, [b]Φ_T, and [c]Φ_Δ in DMSO.

3. Conclusions

CDs have emerged as versatile nanoplatforms capable of addressing key limitations associated with molecular compounds such as Pcs. By combining CDs with Pcs, the resulting hybrid macrocycles exhibit improved light sensitivity, water solubility, stability, and environmental compatibility. This review allows to conclude that this integration can significantly expand the applications of Pcs, with the resulting hybrids showing great promise in diverse fields, including biosensing, phototherapeutic applications, photocatalysis, electrocatalysis, and oxygen reduction reactions (ORR) among others.

Most of the research focused on developing Pcs and CDs with compatible functionalities. This involved tailoring Pcs structural features, such as peripheral substituents (α and/or β), varying the type and number of functional groups, and modulating charge distributions (neutral, positive, or negative). These modifications enabled the resulting hybrids to achieve in general appropriate performance in terms of $\Phi\Delta$, ΦF, photostability, hydrophilicity, and targeted functionality.

The conjugation of CDs with Pc dyes through covalent or non-covalent interactions yielded Pc@CDs hybrids with distinct photophysical properties. Covalent strategies were primarily based on amidation and esterification. The wide structural variety of Pcs facilitated the functionalization of oxygen and nitrogen-containing groups on the CDs. While covalently bonded hybrids exhibit greater chemical stability and higher reaction yields, their practical applications are hindered by synthetic complexity, generally requiring the preparation of non-symmetrical Pcs. Nevertheless, covalent functionalization influences the interaction between the two structures, modulating photoluminescence, preserving the capacity for $^1O_2$ generation and introducing interesting features favorable for mediating electron transfer, conductivity and ORR processes. Although the number of reported examples is limited, we believe that continued efforts to develop this type of hybrids can significantly impact renewable energy technologies, advance environmental sustainability, improve catalytic efficiency, and drive innovations in therapeutic applications. On the other hand, non-covalent conjugation, achieved through electrostatic interactions, complexation, or π–π stacking, facilitates the easy formation of supramolecular structures. Considering that some Pc@CDs hybrids exhibit pH-dependent behavior, prompted some groups to explore electrostatic interactions to optimize Pc–CDs binding. The non-covalent conjugation approach offers the advantage of faster and simpler reaction steps while preserving the structural and electronic characteristics of the starting materials. However, non-covalent strategies generally compromised the photoluminescence of Pc@CDs hybrids due to quenching effects. These quenching effects were extensively explored in sensing applications, where luminescence was recovered upon interaction with the target analyte.

Despite the observed decrease in the fluorescence quantum yield (Φ_F) of the conjugates and the corresponding increase in triplet quantum yield (Φ_T), these changes did not always translate into improved efficiency in generating $^1O_2$ due to competing screening processes that reduce light absorption or oxygen access to the active sites of the photosensitizer. Nevertheless, depending on the structural features of the Pcs, these limitations were overcome in some cases, leading to promising outcomes in PDT and aPDT. The ability to generate ROS was also explored in oxidative processes in water, although the number of studies remains very limited. Similarly, studies related to hydrogen production are scarce.

Despite significant progress, the development of highly efficient Pc@CDs hybrids remains an open research frontier. The primary challenge lies in mitigating the partial or total quenching of Pcs by CDs, an effect observed in both covalent and non-covalent conjugation approaches. This quenching typically results in reduced ΦF values and ROS production, primarily due to Förster resonance energy transfer (FRET), when compared to free-base Pcs. A critical question to address is how to prevent planar coupling between CDs and Pcs. One promising approach involves the exploration of metalated phthalocyanines with bulky aromatic or aliphatic substituents linked by N, O, or S atoms at the peripheral (α- and/or β-). These substituents can introduce steric hindrance to aromatic CDs, thereby minimizing quenching effects. Also, the metalation of Pcs with transition metals that require axial ligands, such as In^{3+}, Ga^{3+}, or Si^{4+}, can further minimize the direct contact between CDs and Pcs, enhancing the overall performance of the hybrid systems.

Another important aspect is the wide range of synthetic approaches and precursors available to produce CDs in the development of Pc@CDs hybrids, which significantly influence their structural and photophysical/photochemical properties. Therefore, ensuring reproducibility and scalability remains a critical challenge. To address this, it is essential to have well-documented and standardized synthetic protocols that provide clear details on reaction conditions, precursor ratios, and processing steps. This will promote reproducibility and comparability across studies. Advanced characterization techniques and quality control measures will also be vital for confirming structural integrity and performance. In this context, emerging technologies like machine learning (ML) and Deep Learning (DL) can offer powerful tools for the optimization and automated identification of new synthetic conditions. By analyzing large datasets, ML and DL can identify patterns, predict material properties, optimize the process and ultimately enabling more efficient synthetic protocols. These approaches have the potential to significantly enhance the performance of these hybrids, unlocking new possibilities for their applications across diverse fields.

Funding

Acknowledgments

Nanoscale Accepted Manuscript

List of abbreviations

0D – zero dimensional

$^1O_2$ – singlet oxygen

2D – two dimensional

6FBPA - bisphenol A hexafluoride

AA – ascorbic acid

AFM – atomic force microscopy

AmGQDs - aminated graphene quantum dots

aPDT - antimicrobial Photodynamic Therapy

Au-IPA - isophthalic electrografted gold electrode

CDs – carbon dots

CNPs – carbonized nanoparticles

CNTs – carbon nanotubes

CPDs – carbonized polymer dots

CQDs – carbon quantum dots

CV – cyclic voltammetry

DA – dopamine

DBN – 1,8-diazabicyclo[5.4.0]undec-7-ene (DBU) or 1,5-diazabicyclo[4.3.0]non-5-ene

DBU – 1,8-diazabicyclo[5.4.0]undec-7-ene

DCC – *N,N'*-Dicyclohexylcarbodiimide

DMAE – 2-dimethylaminoethanol

DMAP – 4-Dimethylaminopyridine

DMF – *N,N'*-dimethylformamide

DMMP – methylphosphonate

DMSO – dimethyl sulfoxide

DPV - differential pulse voltammetry

ds-DNA - double-stranded DNA

EDC – 1-ethyl-3-(3-dimethylaminopropyl)carbodiimide

EIS - electrochemical impedance spectroscopy

EP - epinephrine

EPR – enhanced permeation retention

FRET – Förster resonance energy transfer

FTIR – Fourier transform infrared spectroscopy

GCE - glassy carbon electrode

GO – graphene oxide

GQDs – graphene quantum dots

H_2Pc – free-base Phthalocyanine

HFIP - hexafluoroisopropanol

ICT – inter charge transfer

IPCA – 5-oxo-1,2,3,5-tetrahydroimidazo-[1,2-α]-pyridine-7-carboxylic acid

LOD - limits of detection

MCF-7 cell lines – human breast cancer cell lines

MPc – metalophthalocyanine

MW – microwave treatment

NCNDs - *N*-doped carbon nanodots

NCDs - nitrogen doped-carbon dots

NHS - *N*-Hydroxysuccinimide

NMR – Nuclear Magnetic Resonance

NOR - norepinephrine

NSCDs - nitrogen-sulfur doped-carbon dots

ORR - oxygen reduction reaction

PACT – photodynamic antimicrobial chemotherapy

PBS – phosphate-buffered saline

Pc(s) – phthalocyanine(s)

PDT – photodynamic therapy

PET – photo-induced electron transfer

PL – photoluminescence

Por – porphyrin

QY – quantum yield

rGQDs - reduced graphene quantum dots

SDT - sonodynamic therapy

SEC – spectroelectrochemistry

SEM – scanning electron microscopy

SWV - square wave voltammetry

t-CDs – thermally-reduced carbon dots

TEM – transmission electron microscopy

TEMPOL – 4-hydroxy-2,2,6,6-tetramethylpiperidine-1-oxyl 2,2,6,6 tetramethylpiperidin-1-yl)oxyl

TEMPO-Pht – phthalonitrile bearing the radical scavenger TEMPOL

XPS – X-ray photoelectron spectroscopy

XRD - X-ray diffraction

J – spectral overlap

τ_f – fluorescence lifetime

Φ_F – fluorescence quantum yield

Φ_{PL} – photoluminescence quantum yield

Φ_T – triplet quantum yield

Φ_Δ – singlet oxygen quantum yield

Nanoscale Accepted Manuscript

References

[1]   M. W. Jones, A. I. Coppola, S. H. Doerr, T. A. Quine, C. Santín, T. Dittmar, R. Jaffé, *Nat Commun* **2020**, *11*, 1.

[2]   A. Kelarakis, *Cambridge University Press* **2020**, *1*, 1.

[3]   Q. Xu, W. Li, L. Ding, W. Yang, H. Xiao, W. Ong, *Nanoscale* **2019**, 11, 1475.

[4]   K. Jiang, S. Sun, L. Zhang, Y. Lu, A. Wu, C. Cai, H. Lin, *Angew Chem Int Ed* **2015**, 127, 5450.

[5]   L. Đorđević, F. Arcudi, M. Cacioppo, M. Prato, *Nat Nanotech* **2022**, *17*, 112.

[6]   A. Das, E. V. Kundelev, A. A. Vedernikova, S. A. Cherevkov, D. V. Danilov, A. V. Koroleva, E. V. Zhizhin, A. N. Tsypkin, A. P. Litvin, A. V. Baranov, A. V. Fedorov, E. V. Ushakova, A. L. Rogach, *Light Sci Appl* **2022**, *11*, 1.

[7]   Q. Zhang, R. Wang, B. Feng, X. Zhong, K. (Ken) Ostrikov, *Nat Commun* **2021**, *12*, 1.

[8]   B. Bartolomei, A. Bogo, F. Amato, G. Ragazzon, M. Prato, *Angew Chem Int Ed* **2022**, 61, e202200038.

[9]   S. Hu, A. Trinchi, P. Atkin, I. Cole, *Angew Chem Int Ed* **2015**, *54*, 2970.

[10]   G. E. Lecroy, F. Messina, A. Sciortino, C. E. Bunker, P. Wang, K. A. S. Fernando, Y. P. Sun, *J Phys Chem C* **2017**, *121*, 28180.

[11]   F. Yan, Z. Sun, H. Zhang, X. Sun, Y. Jiang, Z. Bai, *Microchimica Acta* **2019**, *186*, 1.

[12]   H. Ali, S. Ghosh, N. R. Jana, *Wiley Interdiscip Rev Nanomed Nanobiotechnol* **2020**, *12*, e1617.

[13]   J. Zhu, S. Mu, *Adv Funct Mater* **2020**, *30*, 2001097.

[14]   Y. P. Sun, B. Zhou, Y. Lin, W. Wang, K. A. S. Fernando, P. Pathak, M. J. Meziani, B. A. Harruff, X. Wang, H. Wang, P. G. Luo, H. Yang, M. E. Kose, B. Chen, L. M. Veca, S. Y. Xie, *J Am Chem Soc* **2006**, *128*, 7756.

[15]   X. T. Tian, X. B. Yin, *Small* **2019**, *15*, 1901803.

[16]   Z. Wang, F. Yuan, X. Li, Y. Li, H. Zhong, L. Fan, S. Yang, *Adv Mater* **2017**, *29*, 1702910.

[17]   D. Li, P. Jing, L. Sun, Y. An, X. Shan, X. Lu, D. Zhou, D. Han, D. Shen, Y. Zhai, S. Qu, R. Zbořil, A. L. Rogach, *Adv Mater* **2018**, *30*, 1705913.

[18]   M. T. Hasan, R. Gonzalez-Rodriguez, C. Ryan, N. Faerber, J. L. Coffer, A. V. Naumov, *Adv Funct Mater* **2018**, *28*, 1804337.

[19]   B. Ju, H. Nie, Z. Liu, H. Xu, M. Li, C. Wu, H. Wang, S. X. A. Zhang, *Nanoscale* **2017**, *9*, 13326.

[20]   H. Nie, M. Li, Q. Li, S. Liang, Y. Tan, L. Sheng, W. Shi, S. X. A. Zhang, *Chem Mater* **2014**, *26*, 3104.

[21]   H. Ding, J. S. Wei, P. Zhang, Z. Y. Zhou, Q. Y. Gao, H. M. Xiong, *Small* **2018**, *14*, 1800612.

[22]   S. Miao, K. Liang, J. Zhu, B. Yang, D. Zhao, B. Kong, *Nano Today* **2020**, *33*, 100879.

[23]   X. Li, Y. Fu, S. Zhao, J. F. Xiao, M. Lan, B. Wang, K. Zhang, X. Song, L. Zeng, *Chem Eng J* **2022**, *430*, 133101.

[24]   S. Yoo, Y. Song, S. Hahn, *Light Sci Appl 2022 11:1* **2022**, *11*, 1.

Nanoscale Accepted Manuscript

[25] J. Tang, J. Zhang, Y. Zhang, Y. Xiao, Y. Shi, Y. Chen, L. Ding, W. Xu, *Nanoscale Res Lett* **2019**, *14*, 1.

View Article Online
DOI: 10.1039/D5NR00466G

[26] M. Bottrill, M. Green, *Chem Commun* **2011**, *47*, 7039.

[27] K. M. Tsoi, Q. Dai, B. A. Alman, W. C. W. Chan, *Acc Chem Res* **2013**, *46*, 662.

[28] L. Ye, K. T. Yong, L. Liu, I. Roy, R. Hu, J. Zhu, H. Cai, W. C. Law, J. Liu, K. Wang, J. Liu, Y. Liu, Y. Hu, X. Zhang, M. T. Swihart, P. N. Prasad, *Nat Nanotech 2012 7:7* **2012**, *7*, 453.

[29] A. M. Derfus, W. C. W. Chan, S. N. Bhatia, *Nano Lett* **2004**, *4*, 11.

[30] Z. L. Wu, Z. X. Liu, Y. H. Yuan, *J Mater Chem B* **2017**, *5*, 3794.

[31] F. Arcudi, L. Ðorđević, M. Prato, *Acc Chem Res* **2019**, *52*, 2070.

[32] F. Arcudi, L. Ðorđević, F. Arcudi, L. Ðorđević, *Small* **2023**, *19*, 2300906.

[33] L. Ðorđević, F. Arcudi, M. Prato, *Nat Protoc* **2019**, *14*, 2931.

[34] Y. Dong, J. Shao, C. Chen, H. Li, R. Wang, Y. Chi, X. Lin, G. Chen, *Carbon N Y* **2012**, *50*, 4738.

[35] I. L. Medintz, H. T. Uyeda, E. R. Goldman, H. Mattoussi, *Nat Mater 2005 4:6* **2005**, *4*, 435.

[36] H. Zhu, X. Wang, Y. Li, Z. Wang, F. Yang, X. Yang, *Chem Commun* **2009**, 5118.

[37] H. Peng, J. Travas-Sejdic, *Chem Mater* **2009**, *21*, 5563.

[38] D. V. Talapin, A. L. Rogach, E. V. Shevchenko, A. Kornowski, M. Haase, H. Weller, *J Am Chem Soc* **2002**, *124*, 5782.

[39] P. C. Yibo Yan, Dong Zhai, Yi Liu, Jun Gong, Jie Chen, Ping Zan, Zhiping Zeng, Shuzhou Li, Wei Huang*, *ACS Nano* **2018**, *12*, 3523.

[40] J. Schneider, C. J. Reckmeier, Y. Xiong, M. Von Seckendorff, A. S. Susha, P. Kasak, A. L. Rogach, *J Phys Chem C* **2017**, *121*, 2014.

[41] F. Yuan, Y. K. Wang, G. Sharma, Y. Dong, X. Zheng, P. Li, A. Johnston, G. Bappi, J. Z. Fan, H. Kung, B. Chen, M. I. Saidaminov, K. Singh, O. Voznyy, O. M. Bakr, Z. H. Lu, E. H. Sargent, *Nature Photon 2019 14:3* **2019**, *14*, 171.

[42] L. Wang, Y. Wang, T. Xu, H. Liao, C. Yao, Y. Liu, Z. Li, Z. Chen, D. Pan, L. Sun, M. Wu, *Nature Communications 2014 5:1* **2014**, *5*, 1.

[43] E. Haque, J. Kim, V. Malgras, K. R. Reddy, A. C. Ward, J. You, Y. Bando, Md. S. A. Hossain, Y. Yamauchi, *Small Methods* **2018**, *2*.

[44] C. I. M. Santos, I. F. A. Mariz, S. N. Pinto, G. Gonçalves, I. Bdikin, P. A. A. P. Marques, M. G. P. M. S. Neves, J. M. G. Martinho, E. M. S. Maçôas, *Nanoscale* **2018**, *10*, 12505.

[45] C. I. M. Santos, L. Rodríguez-Pérez, G. Gonçalves, S. N. Pinto, M. Melle-Franco, P. A. A. P. Marques, M. A. F. Faustino, M. Á. Herranz, N. Martin, M. G. P. M. S. Neves, J. M. G. Martinho, E. M. S. Maçôas, *Carbon N Y* **2020**, *166*, 164.

[46] C. I. M. Santos, L. Rodríguez-Pérez, G. Gonçalves, C. J. Dias, F. Monteiro, M. do A. F. Faustino, S. I. Vieira, L. A. Helguero, M. Á. Herranz, N. Martín, M. G. P. M. S. Neves, J. M. G. Martinho, E. M. S. Maçôas, *ACS Appl Nano Mater* **2021**, *4*, 13079.

[47] A. Braun, *J. Ber.*, **1907**, 40, 2709.

[48]   H. von der W. E. Diesbach, *Helvetica Chimica Acta,* **1927**, 10, 886.

[49]   N. B. McKeown, *McKeown, N. B., Ed., Cambridge University Press, Cambridge, UK* **1998**, 1.

[50]   A. L. Thomas, Phthalocyanine Research and Applications, CRC Press, **1990**.

[51]   A. G. Dandridge, H. A. E. Drescher, J. Thomas, *In Dyes*, **1929**, 169.

[52]   J. M. Robertson, *J Chem Soc* **1935**, 615.

[53]   J. M. Robertson, *J Chem Soc* **1936**, 1195.

[54]   R. P. Linstead, J. M. Robertson, *J Chem Soc* **1936**, 1736.

[55]   J. M. Robertson, I. D. A. Woodward, *J Chem Soc* **1937**, 219.

[56]   J. M. Robertson, I. Woodward, *J Chem Soc* **1940**, 36.

[57]   R. P. Linstead, *J Chem Soc* **1934**, 1016.

[58]   G. T. Byrne, R. P. Linstead, A. R. Lowe, *J Chem Soc* **1934**, 1017.

[59]   C. E. Dent, R. P. Linstead, *J Chem Soc* **1934**, 1027.

[60]   C. E. Dent, R. P. Linstead, A. R. Lowe, *J Chem Soc* **1934**, 1033.

[61]   D. Gounden, N. Nombona, W. E. van Zyl, *Coord Chem Rev* **2020**, *420*.

[62]   S. Yang, Y. Yu, X. Gao, Z. Zhang, F. Wang, *Chem Soc Rev* **2021**, *50*, 12985.

[63]   D. Li, S. Cai, P. Wang, H. Cheng, B. Cheng, Y. Zhang, G. Liu, *Adv Healthc Mater* **2023**, *12*.

[64]   T. Furuyama, K. Satoh, T. Kushiya, N. Kobayashi, *J Am Chem Soc* **2014**, *136*, 765.

[65]   H., H. E., N. T., I. H., S. S. Tomoda, in *Chem. Lett.*, **1976**, 1003.

[66]   T. Haruhiko, S. Shojiro, O. Shojiro, S. Shinsaku, *Chem Lett*, **2006**, *9*, 1277.

[67]   S. W. Oliver, T. D. Smith, *J Chem Soc, Perkin Transactions 2* **1987**, 1579.

[68]   P. J., G. S. J., O. O. A., W. L. Brach, *J. Heterocyclic. Chem.* **1970**, *7*, 1403.

[69]   H. J. Callot, F. Metz, C. Piechocki, *Tetrahedron*, **1982**, 38, 2365.

[70]   G., B. G., H. U., T. T. de la Torre, in *Functional Phthalocyanine Molecular Materials*, **2010**, 1–44.

[71]   C. C. Leznoff, M. Hu, K. J. M. Nolan, *Chem Commun* **1996**, 1245.

[72]   J. Follana-Berná, R. Farran, W. Leibl, A. Quaranta, Á. Sastre-Santos, A. Aukauloo, *Angew Chem Int Ed* **2021**, *60*, 12284.

[73]   O. L. Kaliya, E. A. Lukyanets, G. N. Vorozhtsov, *J. Porphyr Phthalocya*, **1999**, 3, 592.

[74]   B. A. Bench, W. W. Brennessel, H.-J. Lee, S. M. Gorun, H. Ali, J. E. van Lier, **2002**, *Angew. Chem. Int. Ed.*, 41, 747

[75]   O. Tsaryova, A. Semioshkin, D. Wöhrle, V. I. Bregadze, *J Porphyr Phthalocya* **2012**, 9, 268.

[76]   X. Duan, Y. Zhang, H. Wang, F. Dai, G. Yang, Y. Chen, *New J Chem* **2020**, *44*, 13240.

[77]   C. P. S., L. L. M. O. Ribeiro, *J. Photochem. Photobiol.* **2021**, *48*, 1.

Nanoscale Accepted Manuscript

[78] S. R. D. Gamelas, A. T. P. C. Gomes, M. A. F. Faustino, A. C. Tomé, J. P. C. Tomé, A. Almeida, L. M. O. Lourenço, *ACS Appl Bio Mater* **2020**, *3*, 4044.

[79] L. Lourenço, D. Rocha, C. Ramos, M. Gomes, A. Almeida, M. Faustino, F. Paz, M. Neves, A. Cunha, J. P. C. Tome, L. M. O. Lourenço, Deisy, M. G. C. Rocha, C. I. V Ramos, M. C. Gomes, M. A. F. Faustino, F. A. Almeida Paz, M. G. P. M. S. Neves, Â. Cunha, J. P. C. Tomé, *ChemPhotoChem* **2019**, 3, 251.

[80] L. M. O. Lourenço, A. Sousa, M. C. Gomes, M. A. F. Faustino, A. Almeida, A. M. S. Silva, M. G. P. M. S. Neves, J. A. S. Cavaleiro, Â. Cunha, J. P. C. Tomé, *Photochem. Photobiol. Sci.* **2015**, *14*, 1853.

[81] K. A. D. F., P. J. A., B. J. C. , T. J. P. C. , da S. R. S., L. L. M. O. Castro, *Front Chem* **2022**, 10, 1.

[82] L. M. O. Lourenço, P. M. R. Pereira, E. Maciel, M. Válega, F. M. J. Domingues, M. R. M. Domingues, M. G. P. M. S. Neves, J. A. S. Cavaleiro, R. Fernandes, J. P. C. Tomé, *Chem Commun* **2014**, *50*, 8363.

[83] L. M. O. Lourenço, M. G. P. M. S. Neves, J. A. S. Cavaleiro, J. P. C. Tomé, *Tetrahedron* **2014**, *70*, 2681.

[84] J. Lopes-Nunes, J. Carvalho, J. Figueiredo, C. I. V. Ramos, L. M. O. Lourenço, J. P. C. Tomé, M. G. P. M. S. Neves, J. L. Mergny, J. A. Queiroz, G. F. Salgado, C. Cruz, *Bioorg Chem* **2020**, *100*.

[85] C. I. V. Ramos, S. P. Almeida, L. M. O. Lourenço, P. M. R. Pereira, R. Fernandes, M. A. F. Faustino, J. P. C. Tomé, J. Carvalho, C. Cruz, M. G. P. M. S. Neves, *Molecules* **2019**, *24*, 733.

[86] L. M. O. Lourenço, B. A. Iglesias, P. M. R. Pereira, H. Girão, R. Fernandes, M. G. P. M. S. Neves, J. A. S. Cavaleiro, J. P. C. Tomé, *Dalton Transactions* **2015**, *44*, 530.

[87] S. Dutta, B. G. Ongarora, H. Li, M. G. H. da Vicente, B. K. Kolli, K. P. Chang, *PLoS One* **2011**, *6*, e20786.

[88] J. M. D. Calmeiro, J. P. C. Tomé, L. M. O. Lourenço, *J Mater Chem C Mater* **2020**, *8*, 8344.

[89] L. Wibmer, L. M. O. Lourenço, A. Roth, G. Katsukis, M. G. P. M. S. Neves, J. A. S. Cavaleiro, J. P. C. Tomé, T. Torres, D. M. Guldi, *Nanoscale* **2015**, *7*, 5674.

[90] L. M. O. Lourenço, A. Hausmann, C. Schubert, M. G. P. M. S. Neves, J. A. S. Cavaleiro, T. Torres, D. M. Guldi, J. P. C. Tomé, *Chempluschem* **2015**, *80*, 832.

[91] L. C. Nene, T. Nyokong, *Diam Relat Mater* **2023**, *131*, 109549.

[92] B. Uprety, H. Abrahamse, *Front Chem* **2022**, *10*.

[93] L. Lei, B. Dai, T. Han, C. Zhou, Z. Gong, P. Zhang, *Front Mater* **2022**, *9*, 744.

[94] X. Xu, R. Ray, Y. Gu, H. J. Ploehn, L. Gearheart, K. Raker, W. A. Scrivens, *J Am Chem Soc* **2004**, *126*, 12736.

[95] C. Xia, S. Zhu, T. Feng, M. Yang, B. Yang, C. Xia, T. Feng, M. Yang, B. Yang, S. Zhu, *Adv Sci* **2019**, *6*, 1901316.

[96] D. Yakovlev, E. Kolesova, S. Sizova, K. Annas, M. Tretyak, V. Loschenov, A. Orlova, V. Oleinikov, *Nanomaterials* **2022**, *12*, 3874.

[97] A. C. S. Samia, X. Chen, C. Burda, *J Am Chem Soc* **2003**, *125*, 15736.

[98] Ş. Eryiğit, A. Gelir, E. Budak, C. Ünlü, A. Gömleksiz, İ. Özçeşmeci, A. Gül, *Luminescence* **2022**, *37*, 268.

Nanoscale Accepted Manuscript

[99] L. Fan, Y. Hu, X. Wang, L. Zhang, F. Li, D. Han, Z. Li, Q. Zhang, Z. Wang, L. Niu, *Talanta* **2012**, *101*, 192.

[100] O. J. Achadu, I. Uddin, T. Nyokong, *J Photochem Photobio A: Chem*, **2016**, 317, 12.

[101] I. Scalise, E. N. Durantini, *Bioorg Med Chem* **2005**, 13, 3037.

[102] Md. K. Nazeeruddin, R. Humphry-Baker, M. Grätzel, Md. K. Nazeeruddin, R. Humphry-Baker, M. Grätzel, B. A. Murrer, *Chemical Communications* **1998**, 719.

[103] O. J. Achadu, T. Nyokong, *New J Chem* **2016**, *40*, 8727.

[104] S. Eken Korkut, D. Akyüz, K. Özdo1an, Y. Yerli, A. Koca, M. K. Şener, *Dalton Trans* **2016**, *45*, 3086.

[105] O. J. Achadu, T. Nyokong, *J Fluoresc* **2016**, *26*, 283.

[106] A. Ogunsipe, J. Y. Chen, T. Nyokong, *New J Chem* **2004**, *28*, 822.

[107] O. J. Achadu, T. Nyokong, *Talanta* **2017**, *166*, 15.

[108] O. J. Achadu, T. Nyokong, *Dyes Pigm* **2017**, *145*, 189.

[109] O. J. Achadu, T. Nyokong, *Dyes Pigm* **2019**, *160*, 328.

[110] W. Jiang, M. Jiang, T. Wang, X. Chen, M. Zeng, J. Yang, Z. Zhou, N. Hu, Y. Su, Z. Yang, *RSC Adv* **2021**, *11*, 14805.

[111] W. Jiang, X. Chen, T. Wang, B. Li, M. Zeng, J. Yang, N. Hu, Y. Su, Z. Zhou, Z. Yang, *RSC Adv* **2021**, *11*, 5618.

[112] A. M. Santiago, C. I. M. Santos, L. M. O. Lourenço, I. F. A. Mariz, J. P. C. Tomé, E. Maçôas, *Nanomaterials* **2022**, *12*, 1892.

[113] O. J. Achadu, T. Nyokong, *Dyes Pigm* **2019**, *160*, 328.

[114] S. M. Mousavi, M. Y. Kalashgrani, N. Javanmardi, M. Riazi, M. H. Akmal, V. Rahmanian, A. Gholami, W. H. Chiang, *J Mater Chem B* **2024**, *12*, 7041.

[115] A. Karagianni, N. G. Tsierkezos, M. Prato, M. Terrones, K. V. Kordatos, *Carbon N Y* **2023**, *203*, 273.

[116] R. Matshitse, K. E. Sekhosana, O. J. Achadu, T. Nyokong, *J Coord Chem* **2017**, *70*, 3308.

[117] T. Fan, W. Zeng, W. Tang, C. Yuan, S. Tong, K. Cai, Y. Liu, W. Huang, Y. Min, A. J. Epstein, *Nanoscale Res Lett* **2015**, *10*, 1.

[118] N. Nwahara, R. Nkhahle, B. P. Ngoy, J. Mack, T. Nyokong, *New J Chem* **2018**, *42*, 6051.

[119] L. C. Nene, M. E. Managa, D. O. Oluwole, D. M. Mafukidze, A. Sindelo, T. Nyokong, *Inorganica Chim Acta* **2019**, *488*, 304.

[120] R. Matshitse, T. Nyokong, *J Fluoresc* **2018**, *28*, 827.

[121] L. C. Nene, M. Managa, T. Nyokong, *Dyes Pigm* **2019**, *165*, 488.

[122] R. Matshitse, N. Nwaji, M. Mananga, E. Prinsloo, T. Nyokong, *J Photochem Photobiol A Chem* **2018**, *367*, 253.

[123] M. De, S. Ghosh, T. Sen, M. Shadab, I. Banerjee, S. Basu, N. Ali, *Mol Ther Nucleic Acids* **2018**, *10*, 9.

Nanoscale Accepted Manuscript

[124] G. van der Horst, A. F. van de Merbel, E. Ruigrok, M. H. van der Mark, E. Ploeg, L. Appelman, S. Tvingsholm, M. Jäätelä, J. van Uhm, M. Kruithof-de Julio, G. N. Thalmann, R. C. M. Pelger, C. H. Bangma, J. L. Boormans, G. van der Pluijm, E. C. Zwarthoff, *Mol Oncol* **2020**, *14*, 3121.

[125] L. C. Nene, T. Nyokong, *Photodiagnosis Photodyn Ther* **2021**, *36*, 102573.

[126] K. Celep, G. Gökçil, P. Şen, F. Şahin, A. Erdoğmuş, G. Y. Atmaca, *Appl Organomet Chem* **2025**, *39*, e70007.

[127] G. Gökçil, G. Y. Atmaca, P. Şen, F. Şahin, A. Erdoğmuş, *J Photochem Photobiol A Chem* **2025**, *459*, 116108.

[128] G. Gökçil, K. Celep, P. Şen, F. Şahin, A. Erdoğmuş, G. Y. Atmaca, *Polyhedron* **2025**, *272*, 117468.

[129] Y. I. Openda, P. Sen, M. Managa, T. Nyokong, *Photodiagnosis Photodyn Ther* **2020**, *29*, 101607.

[130] L. Hui, J. Huang, G. Chen, Y. Zhu, L. Yang, *ACS Appl Mater Interfaces* **2016**, *8*, 20.

[131] P. M. Sivakumar, G. Sheshayan, M. Doble, *Chem Biol Drug Des* **2008**, *72*, 303.

[132] P. Sen, N. Nwahara, T. Nyokong, *Main Group Chemistry* **2021**, *20*, 175.

[133] M. Özçeşmeci, S. Gümrükçü, C. Ünlü, İ. Y. Coşkun, S. Özdemir, M. S. Yalçın, G. Tollu, İ. Özçeşmeci, *Appl Organomet Chem* **2024**, *38*, e7423.

[134] D. M. Mafukidze, T. Nyokong, J Coord Chem **2017**, *70*, 3598.

[135] O. J. Achadu, M. Managa, T. Nyokong, *J Photochem Photobiol A Chem* **2017**, *C*, 174.

[136] Q. Chen, Y. Liu, B. Mao, Z. Wu, W. Yan, D. Zhang, Q. Li, H. Huang, Z. Kang, W. Shi, *Adv Funct Mater* **2023**, *33*, 2305318.

[137] S. A. Majeed, N. Nwaji, J. Mack, T. Nyokong, S. Makhseed, *J Lumin* **2019**, *213*, 88.

[138] D. AlMarzouq, S. A. Majeed, Ö. Budak, A. Koca, *Inorganica Chim Acta* **2021**, *527*, 120558.

[139] M. Cacioppo, T. Scharl, L. Đorđević, A. Cadranel, F. Arcudi, D. M. Guldi, M. Prato, Angew. Chem. Int. Ed. **2020**, *59*, 12779.

[140] D. M. Mafukidze, T. Nyokong, *J Mol Struct* **2019**, *1180*, 307.

[141] S. Centane, E. K. Sekhosana, R. Matshitse, T. Nyokong, *J. Electroanal. Chem.* **2018**, *820*, 146.

[142] H. M. Sharma, D. K. Das, A. Kumar, *Int J Hydrogen Energy* **2024**, *110*, 159.

[143] K. H. Koh, S. H. Noh, T. H. Kim, W. J. Lee, S. C. Yi, T. H. Han, *RSC Adv* **2017**, *7*, 26113.

[144] Y. Lu, Y. Jiang, X. Gao, X. Wang, W. Chen, *J Am Chem Soc* **2014**, *136*, 11687.

[145] C. Luhana, I. Moyo, K. Tshenkeng, P. Mashazi, *Microchem J* **2022**, *180*, 107605.

Nanoscale Accepted Manuscript

Data available statement

From: Gil Gonçalves
University of Aveiro
Centre for Mechanical Technology and Automation (TEMA)
Department of Mechanical Engineering
Campus Universitario de Santiago
3810-193 Aveiro
Portugal
e-mail: ggoncalves@ua.pt

To the Editor of Nanoscale,

No primary research results, software or code have been included and no new data were generated or analysed as part of this review **"Carbon dots-phthalocyanine hybrids: synergistic effects that boost their multifaceted applications"**.
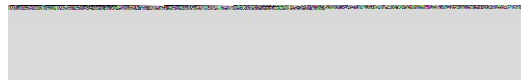
On behalf of all authors

Yours sincerely,

10 April 2025, Aveiro

(Gil Gonçalves)

Nanoscale Accepted Manuscript